SUPPLEMENTARY INFORMATION

Excitatory Dysfunction Drives Network and Calcium Handling Deficits in 16p11.2 Duplication Schizophrenia Induced Pluripotent Stem Cell-Derived Neurons

Parnell *et al.*

Contents

Supplemental Discussion

A role for excitatory dysfunction in the presentation of activity-dependent and SCZ-relevant phenotypes.

Genetic mapping of SCZ risk loci onto brain cell expression patterns indicate an enrichment within both cortical pyramidal and inhibitory neurons (1). While excitatory deficits have been proposed to participate in SCZ etiology (2), brain imaging (3) and post-mortem GABAergic marker expression (2) studies have implicated impaired GABAergic input as a contributing factor in the presentation of intermediate phenotypes. GABAergic neurons act to regulate excitatory activity and network formation, and altered network synchrony within the cortex is a consistent finding in SCZ patients (4-6). Moreover, deregulated GABA signaling in 16p11.2 duplication animal models has been reported (7). Therefore, a major goal in elucidating the roots of SCZ pathogenesis is to determine the primary cellular locus of genetic dysfunction.

MEAs facilitated in-depth longitudinal phenotyping of iNs in terms of activity and network development. We observed electrical activity deficits, present in both the presence (Fig 1) the absence (Fig 2) of inhibitory neurons, implicating excitatory dysfunction in 16p11.2 duplication-dependent neurodevelopment, supported by recent independent observations (8). This finding appears to be at odds with impaired inhibitory input reported in 16p11.2 duplication mice (7), and SCZ *post mortem* (9-11) and clinical studies (3-5, 12). However, altered neuronal activity has been reported in idiopathic SCZ iN, where SCZ-iNs showed firing deficits with few inhibitory neurons present (13). Interestingly, iGN were observed to repress firing rate and network bursting in iGN/iEN cocultures (Fig S4) and iEN/iGN DUP cocultures failed to show significant alterations in firing rate or synchrony until 7WIV (Fig 1), as opposed to 5WIV in iEN cultures (Fig 2). This observation suggests that the presence of iGN may mask excitatory neuron deficits in iEN/iGN cocultures at these earlier time points. Although iGN specific deficits may contribute to neuronal dysfunction, assessment of this is made more challenging by the poor development of iGN in

monoculture (data not shown). While it is tempting to hypothesize that excitatory deficits early in development may result in inhibitory neuron compensation and E/I imbalance later in development (2, 14), further work is required to assess the reciprocal nature of E/I balance in developing SCZ iEN/iGN. In addition, it remains to be seen whether specific GABAergic subtype impairments are present following 16p11.2 duplication. Indeed, PV neurons are sparse within the presented iGN differentiation technique (15). The role of PV neurons in regulating E/I balance and the observation of PV neuron dysfunction in SCZ (2) suggest that studies lacking this cell type may be unable to recapitulate the full neurodevelopmental profile of SCZ. As such, methods to enrich PV content in iPSC-derived cultures may be required to assess their role in SCZ pathophysiology.

A role for genetic background and/or sex in the presentation of 16p11.2 duplication iEN deficits.

Most studies of this CNV have employed 16p11.2 duplication murine models, engineered to duplicate a region of chromosome 7 homologous to the human 16p11.2 locus (reviewed in (16)). However, differences in 16p11.2 duplication phenotypic presentation have been noted depending on murine strain (16), suggesting that the presence and extent of 16p11.2 duplication phenotypes are highly dependent on genetic background. Several phenotypes differed between our isogenic and SCZ patient lines; resting calcium levels, calcium event amplitude (Fig S8A,B vs S19A,B) and Syn1 puncta density (Fig 3E vs 5D), suggesting that additional mechanisms in SCZ backgrounds may amplify or mitigate 16p11.2 duplication-dependent deficits. For example, whereas we found no alterations in Syn1 density in isogenic lines, SCZ patients showed robust deficits suggesting a potential amplification of presynaptic dysfunction due to convergent genetic effects. It is noteworthy that previous observations have found reduced synaptic connections (8, 17, 18) in isogenic and 16p11.2 duplication lines from mixed diagnosis carriers (see Fig S21). One potential explanation for this disparity is that other studies have assessed pre- and post-

synaptic marker overlap and found significantly reduced synaptic numbers, whereas we assessed only presynaptic content. In support of the validity of this finding, a previous study also found no change in Syn1 density in 16p11.2 duplication (18). It is therefore likely that presynaptic function may be impaired in duplication cells, but the number of sites is unchanged. Alterations in presynaptic function may in turn lead to altered post-synaptic changes, supported by our observation of downregulated expression of post-synaptic membrane proteins (Fig 2I) and reported changes in pre/post dual labelled synaptic sites. It is also interesting to note that SCZ patient iENs showed reduced Syn1 puncta, suggesting a conserved effect of genetic factors outside of the CNV in reducing presynaptic content. As such, our results and those of others (17, 19) may be consistent with reduced dendritic spine density observed within the cortex of *post mortem* SCZ brains (20, 21) and reduced connectivity in idiopathic SCZ iN (22).

Of particular interest, a female SCZ 16p11.2 duplication carrier (SCZ2) with low polygenic risk (Fig S9A) showed unaltered firing rate and synchrony, compared to controls (Fig S10), suggesting that sex or genetic background may be important factors in the presentation of 16p11.2 duplication phenotypes. Indeed, background genetic factors have been proposed to explain the variable penetrance and expressivity of the 16p11.2 duplication in clinical cohorts (23), and previous patient iN studies have not assessed polygenic risk for NDDs (17, 18). Moreover, multiple previous studies have employed male patient/isogenic lines (8, 18, 19), and the only study to employ a female 16p11.2 duplication patient did not present phenotypic alterations between patients. Our results suggest that sex may be an important factor in the presentation of 16p11.2 duplication phenotypes, and the possibility of sex-dependent phenotypic presentation is compelling considering the variation in rate, presentation and age of SCZ diagnosis between male and female patients (reviewed in (24, 25)), the observation of male bias in OCD (26) and microcephaly (27) diagnoses in 16p11.2 duplication carriers, and inconsistency in animal model phenotypic presentation (16). However, larger cohorts are required to conclusively determine the

effects of polygenic risk and sex-specific responses in SCZ 16p11.2 duplication carriers. It is also interesting to note the high degree of similarity in morphological (previously reported in (8, 17)) deficits in isogenic and SCZ patient lines, suggesting the 16p11.2 duplication confers robust alterations to neuroarchitecture. Moreover, network activity may be functionally linked to the impaired dendritic length observed, by reducing the expansiveness of neuronal connections, thereby limiting network size and strength (28). 16p11.2 duplication may therefore contribute to SCZ progression via impaired network connectivity, possible linked to altered expression of "Homophilic cell adhesion" genes.

Enrichment in "Homophilic cell adhesion" molecules suggests a potential etiological mechanism underlying observed phenotypes.

We found multiple downregulated DEGs, in both SCZ and isogenic iENs, within the tern "Homophilic cell adhesion". Interestingly, this GO term is enriched in SCZ (29) and previous 16p11.2 duplication RNA-seq data sets (Figs 2, 4, S17, (30)). Isolated DEGs included protocadherins, such as PCDH2, previously observed to be dysregulated in SCZ iEN (31). Protocadherins, and other cell adhesion molecules can regulate neurite outgrowth and synapse stabilization, suggesting a possible mechanism underlying duplication-dependent deficits. It is noteworthy that previous observations have found reduced synaptic connections (17, 19) in isogenic and patient 16p11.2 duplication lines, but not Syn1 density (18), suggesting that functional synapse formation or post-synaptic protein expression may be altered, consistent with our observation of downregulated "Post-synaptic membrane" transcripts (Fig 2I). We therefore hypothesize that cell adhesion molecule-mediated synaptogenesis and presynaptic function may be impaired in duplication neurons, in line with altered expression of cell adhesion molecules and of presynaptic vesicular machinery such as SV2A, STX1B, VGAT (isogenic, Fig S5E) and SV2B, SYT1, UNC13b (patient, Fig S11H). Thus altered connectivity may contribute to network deficits observed, as well as to SCZ progression.

Dysregulation of Calcium homeostasis as a potential underlying mechanism in SCZ

The involvement of calcium-mediated synaptic plasticity in SCZ is supported by exome sequencing studies that revealed high risk *de novo* mutations within VGCC-encoding genes (32, 33) and their regulatory interactors, alongside calcium-permeable NMDAr subunits (34, 35). Further validation of impaired calcium homeostasis stems from *post mortem* transcriptomic and proteomic studies, which have found “Calcium ion binding” to be the most significantly altered gene set within the SCZ brain (36), with a particular enrichment in the calcium-responsive vesicular transport system (37, 38). In addition, altered calcium dynamics have been observed in numerous murine (39-42) and iPSC models of SCZ (43-45).

The observed enrichment of dysregulated SCZ risk genes (Fig S5A-D, S11C-F) in isogenic and patient lines supports 16p11.2 duplication as a driver of SCZ-relevant dysfunction. Isogenic 16p11.2 duplication neurons displayed reductions in firing rate similar to those observed in idiopathic SCZ iN (13), suggesting common SCZ-relevant etiological mechanisms. We found altered expression of “Calcium ion binding” and “Synaptic vesicle release” gene sets, as a common molecular phenotype in isogenic and patient-derived neurons, and in previous 16p11.2 duplication transcriptomic data sets (Fig S17). Both network activity and gene expression changes in duplication SCZ patients coincided with deficits in neuronal calcium dynamics; 16p11.2 duplication calcium events were shorter (Fig 3F, 5F) possibly due to enhanced calcium extrusion. A previous report observed increased outward potassium currents in response to positive voltages in duplication iN (17). Reduced calcium event duration may be linked to altered potassium extrusion, with possible implications for repolarization and observed firing rates deficits. Calcium signaling plays a key role in synaptic plasticity (46), and deficits in calcium homeostasis and gene expression have been reported in SCZ models (13, 22, 42-44, 47), and post-mortem studies (36). It is therefore compelling to hypothesize that impairments in calcium

signaling may limit synaptic plasticity and the functional development of neuronal networks, contributing to the observed network deficits.

Comparison and contrast with previous 16p11.2 duplication studies

Notably, this is the first study to employ 16p11.2 duplication carriers with a SCZ diagnosis, with previous studies using mixed diagnosis 16p11.2 carriers (17), focusing on patients with robust micro/macrocephaly but with mixed co-morbidities (Fig S21, (18)), or employing the same isogenic 16p11.2 duplication lines employed here (8, 19).

Observed 16p11.2 duplication-dependent activity/network phenotypes were strongly corroborated by a recent report employing a matching differentiation protocol and isogenic cell lines (Fig S21, (8)), supporting the validity of our findings; Tai and colleagues found similar deficits in 16p11.2 duplication isogenic iEN, although in their study this phenotype emerged 1 week earlier (8), perhaps linked to higher iEN seeding density on MEAs. Interestingly, studies in dopaminergic neurons and mixed diagnosis 16p11.2 duplication carriers found no alteration in firing rate and network properties (17, 19). It is notable that despite the same isogenic lines being employed by Sundberg and colleagues, both studies employed differentiation methods distinct to both our study and Tai et al, 2022, suggesting that the purity of excitatory neurons, or their maturity, may impact the presentation of activity-dependent phenotypes. Both isogenic and patient-derived iENs displayed aberrant neuroarchitecture manifested as a reduction in dendritic length, consistent with previous reports employing 16p11.2 duplication iNs with mixed diagnoses (17) and isogenic lines (8). This overlap in dendrite length deficits in multiple studies represents a consistent finding, with strong disease relevance, considering the observation of impaired dendritic branching and length observed in the post-mortem SCZ cortex (48).

Supplemental Methods

iPSC derivation and culture

All patient-derived CPLs were reprogrammed by Sendai virus at Rutgers University Cell and DNA Repository (RUCDR)-NIMH Stem Cell Center. All patient lines exhibited successful reprogramming, confirmed by FACs analysis (OCT4/Tra-1-60 double positivity >95%, Fig S9B). Subsequent validation was performed by immunofluorescence staining for pluripotency markers OCT4, SSEA4, NANOG and TRA-1-60. 16p11.2 duplications were confirmed by CNV analysis using Illumina Human Omniexpress and analyzed using GenomeStudio (v2011.1) with CNV Partition (v3.2.0).

iPSCs were cultured in mTeSR (Stemcell Technologies, 85850) and all differentiations were performed between passages 10 and 50. iPSCs were grown on Matrigel Matrix (Corning, 354277). Cells were fed and checked daily for necrotic colony formation, differentiation and general health. Cell passage was performed by Accutase (Millipore Sigma, A6964) or 0.5 mM EDTA (Invitrogen, 15575020). Accutase dissociated cells were plated with 5 μM Y2763, removed during subsequent feeding. MycoAlertPLUS detection kit (Lonza, LT07-118) was used to ensure cells were mycoplasma contamination-free.

Polygenic risk scoring

Polygenic risk was assessed based on SNP microarray of patient as previously reported (49). In brief, we used PRSice to conduct a standard PRS analysis. Pd was the p values of the GWAS study in the discovery sample. ‘significant’ SNPs with Pd<0.5 were pruned based on linkage disequilibrium (LD) ($r2 < 0.2$) in MGS data, and then selected based on seven predetermined significance thresholds (Pd<0.01, 0.05, 0.1, 0.2, 0.3, 0.4, and 0.5) in PGC-SCZ3 (50). Within each pruned SNP set under each significance threshold, a quantitative aggregate risk score was calculated for each individual in the target samples, defined as a sum across SNPs of the number of reference alleles (0, 1, or 2) at that SNP multiplied by the effect size measures (log of OR) for

that SNP estimated from the discovery sample. Association of aggregate risk score and actual SZ in the target samples were performed with logistic regression adjusted for gender, age, and 10 principal components to control for population stratification.

iN differentiation

iENs were induced using lentivirus generated with rtTA (Addgene #20342) and Ngn2 constructs (FUW-TetO-Ngn2-P2A-puromycin, Addgene #52047). 1 day following plating, medium was changed to Neurobasal "complete" (Neurobasal medium (Gibco, #21103049), supplemented with GlutaMAX™ Supplement (1X, Gibco, #35050061), B27 (1X, Gibco, #17504044), N-2 (1X, Gibco, #17502048), MEM Non-Essential Amino Acids Solution (1X, Gibco, #11140050), BDNF (R&D systems, #248-BD), GDNF (R&D systems, #212-GD), NT3 (R&D systems, #267-N3) and Doxycycline (3 µg/mL, Stemgent, #04-2016). DIV2-3 medium contained puromycin (2 µg/mL, Gibco, #A11138-03). Cells were cryopreserved at DIV4 in 45% Growth medium, 45% FBS, 10% DMSO. For coculture studies, iENs were labeled with FUW-TetO-GFP (Addgene #84041).

iGNs were induced using rtTA (as above), Ascl1 and Dlx2 lentivirus constructs (FUW-TetO-Ascl1-T2A-puromycin (Addgene#27150), FUW-TetO-Dlx2-IRES-hygromycin (Addgene #97330)). Selection (DIV2-4) was performed using puromycin (2 µg/mL) and hygromycin (250 µg/mL, Thermofisher #10687010) for three days before retraction and cryopreservation was performed at DIV5. For coculture studies, iGNs were labeled with FUW-TetO-RFP gifted by D. Simkin.

Rat astrocytes

Primary Rat cortical astrocytes (Gibco, N7745100) were cultured as per manufacturer's instructions for 1 passage before cryopreservation in liquid nitrogen. Rat astrocytes were seeded to MEA and coverslips to support all iN cultures.

iN seeding and maintenance

48-well CytoView multi-electrode array (MEA, Axion Biosystems) were matrigel coated at 2x concentration overnight. iEN/iGN were plated at the following concentrations; 1) iENs – 50k iENs 2) iENs/iGNs – 40k iENs, 20k iGNs. All iN were seeded alongside 35k rat astrocytes. For imaging experiments and RNA-sequencing PDL pre-coated coverslips (Neuvitro Corporation, GG-18-15-PDL) were coated with laminin (ThermoFisher #23017015, 1 µg/mL) for one hour. P3 astrocytes were seeded at 75k cells per well (24 well) or 150k (12 well) and grown to confluency for 1-2 days. Feeding was performed 3x weekly by a half medium change for 2 weeks with Neurobasal "complete" (Doxycycline (2 µg/mL), before doxycycline retraction for all subsequent feedings.

Multi-electrode array

MEA plates were read using the Axion Maestro multiwell MEA reader (Axion BiosciENsces) at 37°C with 5% CO_2. 10 minutes of spontaneous activity was recorded using the AxIS 2.5 software (Axion Biosystems). Data analysis; a bandpass filter from 200 Hz to 3 kHz was applied. Spike detection was performed using a threshold of ±6 times the standard deviation of the noise on each electrode. Multielectrode data analysis was performed using the Axion Biosystems Neural Metrics Tool. 5 spikes per second thresholding per electrode was applied. Single electrode bursts were identified as a minimum of five spikes with a maximum interspike interval (ISI_{max}) of 100 milliseconds. Network bursts were identified as a minimum of 10 spikes with an ISI_{max} of 100 milliseconds covered by at least 25% of electrodes in each well (51). The synchrony index was computed through AxIS software, where a value of 0 corresponds to no synchrony while a value of 1 corresponds to perfect synchrony. All data reflects well-wide averages, with the number of wells per condition presented as independent data points. All data presents multiple technical (differentiations) and biological (clone/patient) replicates.

Calcium imaging

At 45-49 DIV, coverslips were transferred to artificial cerebro-spinal fluid (aCSF, in mM: NaCl 125, $NaHCO_3$ 26, glucose 11, KCl 2.5, NaH_2PO_4 1.25, HEPEs 50, $CaCl_2$ 2, $MgCl_2$ 1.25) containing 1 µg/ml Cal520-AM calcium-sensitive fluorogenic dye (AAT Bioquest #21130) for 30 minutes. Coverslips were washed 3x in aCSF and incubated 30 minutes before imaging. Cells were imaged in aCSF for 5-10 minutes at 3FPS, at 37°C at 10x on a C2 Nikon microscope. Depolarization was performed by adding 10x KCl solution (300 mM). Data analysis; image files were exported from NIS elements (Nikon) and analyzed in ImageJ (FIJI) in blind. Cell body regions of interest (ROI) were generated based on a standard deviation max projection image 25 frames before and after KCl stimulation and ROI intensity was measured for each frame. Analysis was performed using a custom MATLAB (r2018a, MATHSWORKS) script. Briefly, data were normalized to a rolling median background (200s). Peaks were detected using the "findpeaks" function with amplitude 10% $\Delta F/F_0$ and duration (>0.5 s, < 2.8 s) thresholds. Cells with no detected events were removed from analysis (with the exception of "% active cells" metric). Averages of all peaks per cell per coverslip were used to generate spontaneous single cell metrics (frequency, amplitude, duration). Resting calcium levels were determined based on the median fluorescence intensity per cell and averaged per coverslip. Network activity was determined using a synchrony threshold based on a random permutation (10,000) of binary coverslip calcium events – synchrony threshold was defined as the average number of events per frame in the randomly shuffled data + 3x standard deviation. Pairwise correlation coefficient (r) was calculated using the Matlab function "corrcoef" for every pair of active cells within the same field of view as a secondary method for assessing neuronal synchrony (1 = 100% traces are perfectly correlated, 0= 0% uncorrelated).

Morphology by Immunofluorescence imaging

45-50 DIV iNs were fixed in 4% Formaldehyde solution in PBS + 4% sucrose (w/v) were permeabilized and stained (52). Coverslips were imaged on a Nikon Ti2 widefield and images

were analyzed in ImageJ. To determine neurite branching and neurite outgrowth, masks were generated by thresholding MAP2 signal and manually separating individual cells. ImageJ neurite outgrowth and Sholl analysis tool were used to generate branching and neurite outgrowth values. Puncta analysis was performed by max entropy autothreshold of Synapsin1 signal and particle detection based on a 0.1-10 μm threshold. Puncta numbers per image were normalized to cell body count within the field of view. All antibodies employed are listed in Table S8.

Total RNA-sequencing and Data analysis

Cells from 2 wells were dissociated from coverslips using Accutase, pooled and spun at 5000xg. Cell pellets were washed with PBS, flash frozen and stored (-80°C). Total RNA extraction was performed as per manufacturer's instructions (mirVANA miRNA isolation kit, Thermofisher, #AM1560). The stranded total RNA-sequencing was conducted and analyzed in the Northwestern University NUSeq Core Facility. RNA quantity was determined with Qubit fluorimeter and total RNA samples were checked for fragment sizing using Agilent Bioanalyzer 2100. The Illumina TruSeq Stranded Total RNA Library Preparation Kit was used to prepare sequencing libraries from 100 ng of total RNA samples. The kit procedure was performed as per manufacturer's instructions. This procedure includes rRNA depletion with RiboZero Gold, cDNA synthesis, 3' end adenylation, adapter ligation, library PCR amplification and validation. Illumina HiSeq 4000 Sequencer was used to sequence the libraries with the production of single-end, 50 bp reads at the sequencing depth of at least 20-25 million reads per sample. The quality of DNA reads, in fastq format, was evaluated using FastQC. Adapters were trimmed, and reads of poor quality or aligning to rRNA sequences were filtered. The reads were also filtered if they aligned to rat (rn6). The cleaned reads were aligned to the human (hg38) genome using STAR (53). Read counts for each gene were calculated using htseq-count (54) in conjunction with a gene annotation file (Ensembl). Normalization and differential expression were determined using DESeq2 (55). The cutoff for determining significantly differentially expressed genes was an FDR-adjusted p-

value<0.1. PPI network was generated using STRING (56) functional clustering with all isogenic significant gene used as input. Clustering was performed using biological process, resulting in 20 attributes and 121 connected nodes. Raw and processed data files are available at GEO (#GSE215183).

Gene ontology analyses

David (57) was employed to isolate significantly deregulated GO terms within FDR<0.1 isogenic and patient 16p11.2 RNA-seq data sets, after removing 16p11.2 genes and X-chromosome genes (within patients to control for male/female expression, no Y DEGs observed). GO analysis was performed for both up and down-regulated gene sets independently. Background was set manually using all expressed genes with mean expression greater than 5 normalized read counts. Significant gene sets were selected using a p-value (FDR)<0.05 cutoff for isogenic, and p<0.05 for patients. Synaptic GO was performed using the SynGO webserver (58) using combined up/downregulated gene lists and including 16p11.2 genes (no significant terms were identified in the absence of 16p11.2, or in independent up/down analyses).

Protein-protein interaction network

All dysregulated genes from isogenic lines (FDR<0.1) were input into the GeneMANIA plugin within Cytoscape to construct a PPI network. Input genes were clustered by biological process (BP) with 50 resultant genes and 20 resultant attributes. The resulting network was assessed for enriched biological processes using DAVID (see Gene ontology analyses).

Gene set enrichment analysis

Gene set enrichment analysis was used to assess the enrichment of disease-relevant genes within the differentially expressed genes of 16p11.2 duplication models. Differentially expressed genes (FDR<0.1) from either isogenic or SZ patient RNA-seq datasets were independently overlapped with gene sets relevant to the genetics of neuropsychiatric disorders. As with gene

ontology analysis, a set of genes expressed in each model (all genes with FPKM>5) was used as the background set (isogenic n= 19569 and SZ patient n= 17343). Only genes within the background sets were included in the analysis. Risk factors associated with neuropsychiatric disorders were obtained from studies of de novo variants and GWAS and lists of genes affected by de novo variants identified in various neuropsychiatric disorders were obtained from Supplemental data compiled in Genovese et al (59) and exome sequencing studies of ASD (60) and SZ (35, 61, 62), as well as to the PyschENCODE list of high confidence SCZ genes (63). Only genes affected by protein-altering variants in probands were included. As a negative control, a list of protein altering *de novo* variants in unaffected siblings was also compiled. For GWAS lists, all protein coding genes predicted to be within GWAS loci were included. A hypergeometric test was used to test for statistical significance of the overlap between altered genes in RNA-seq and disease-relevant gene sets.

iPSC Patient and Clone replication

All experiments were replicated by independent differentiations (immunofluorescence = 2, calcium imaging/MEA=3, with data shown pooled clone/clone, patient/patient data per observation (N=well/coverslip/neuron). Clone by clone and patient by patient data is presented individually in Supplemental files. Biological replication was performed based on the largest source of background variability; for isogenic lines, two clones of a naïve line, and two clones of 16p11.2 duplication isogenic line were differentiated simultaneously to control for genetic alterations during CRISPR-Cas9 modification. For patient lines, 3 healthy and 3 SCZ lines were differentiated simultaneously to control for patient-specific genetic backgrounds. Statistical analysis of DEG overlap was performed by hypergeometric test. For Fig 4N, a patient threshold of FDR<0.3 was employed following observation of many 16p11.2 duplication genes at FDR<0.3. All other comparisons employ FDR<0.1 throughout.

Supplemental Figures

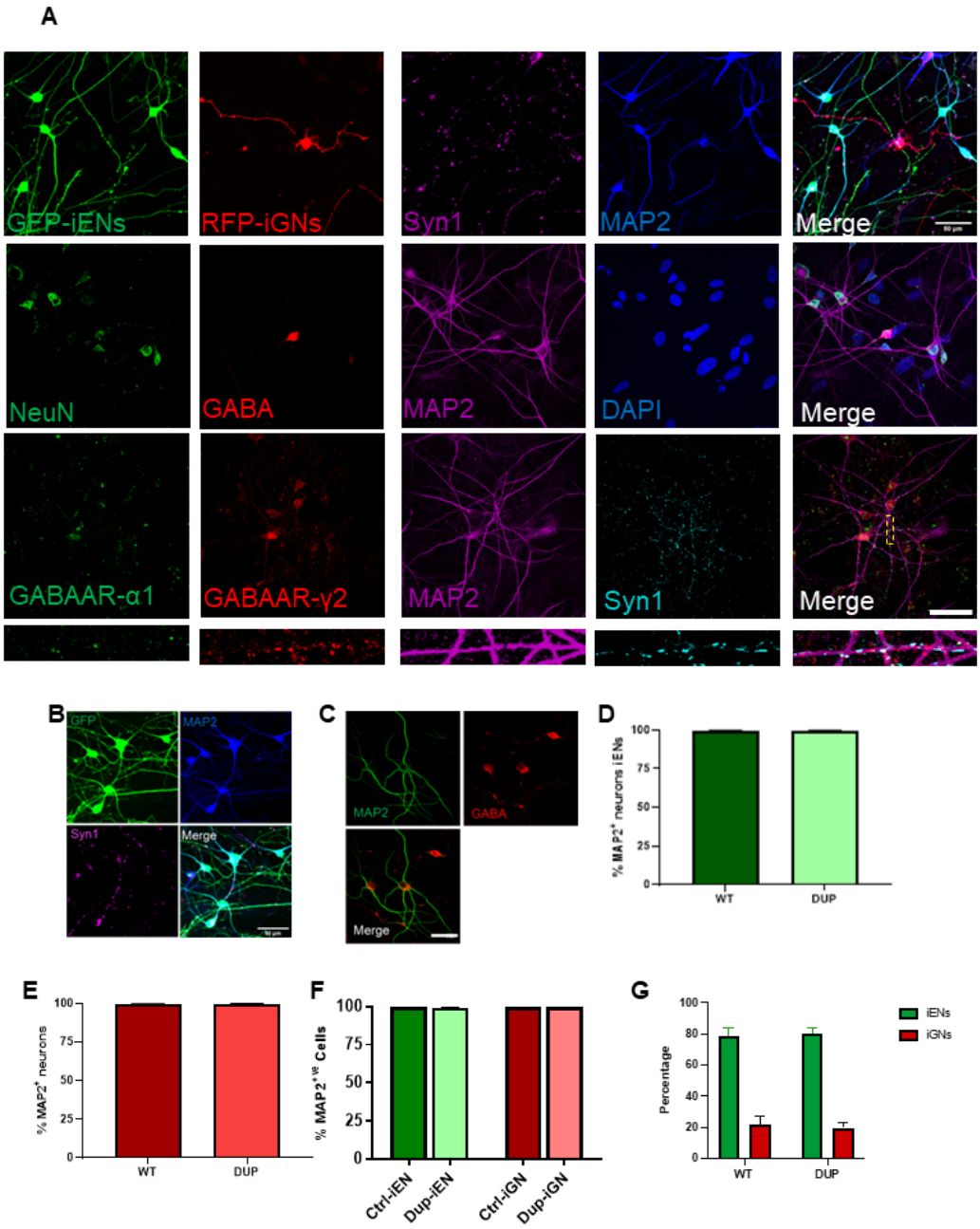

Supplemental Figure 1 – A) Representative image of 7WIV iEN/iGN coculture to assess the presence of neuronal and synaptic markers. Scale bar = 50 μM. Inset shows zoomed region indicated. B) iEN monoculture showing GFP label, stained with MAP2 and Synapsin1. C) iGN monoculture showing MAP2 and GABA. D) Percentage of MAP2 positive GFP-iENs (monoculture). E) Percentage of MAP2 positive RFP-iGNs (monoculture). F) Percentage of MAP2 positive GFP-iENs and RFP-iGNs (coculture). G) Ratio of iENs (green) to iGNs (red) at 7WIV.

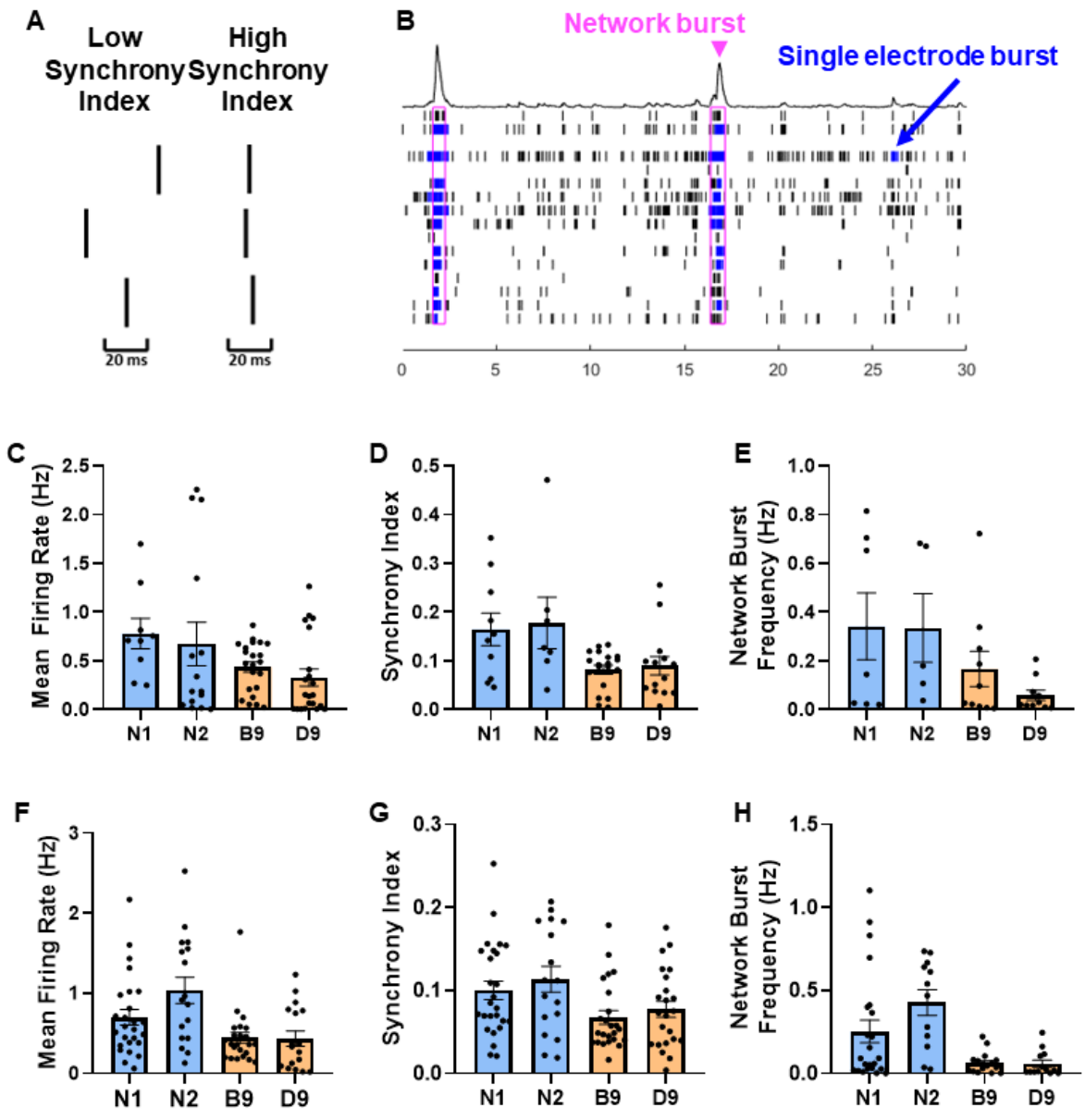

Supplemental Figure 2 – A) Model data showing examples of low and high synchronous firing. B) Model raster plot of network and single electrode bursts highlighted in pink and blue, respectively. C) Mean firing rate of individual clone iEN/iGN cocultures (averaged in Fig 1h). D) Synchrony index of individual clone iEN/iGN cocultures (averaged in Fig 1I). E) Network burst frequency of individual clone iEN/iGN cocultures (averaged in Fig 1J). F) Mean firing rate of individual clone iEN cocultures (averaged in Fig 2E). g) Synchrony index of individual clone iEN cocultures (averaged in Fig 1F). H) Network burst frequency of individual clone iEN cocultures (averaged in Fig 1G).

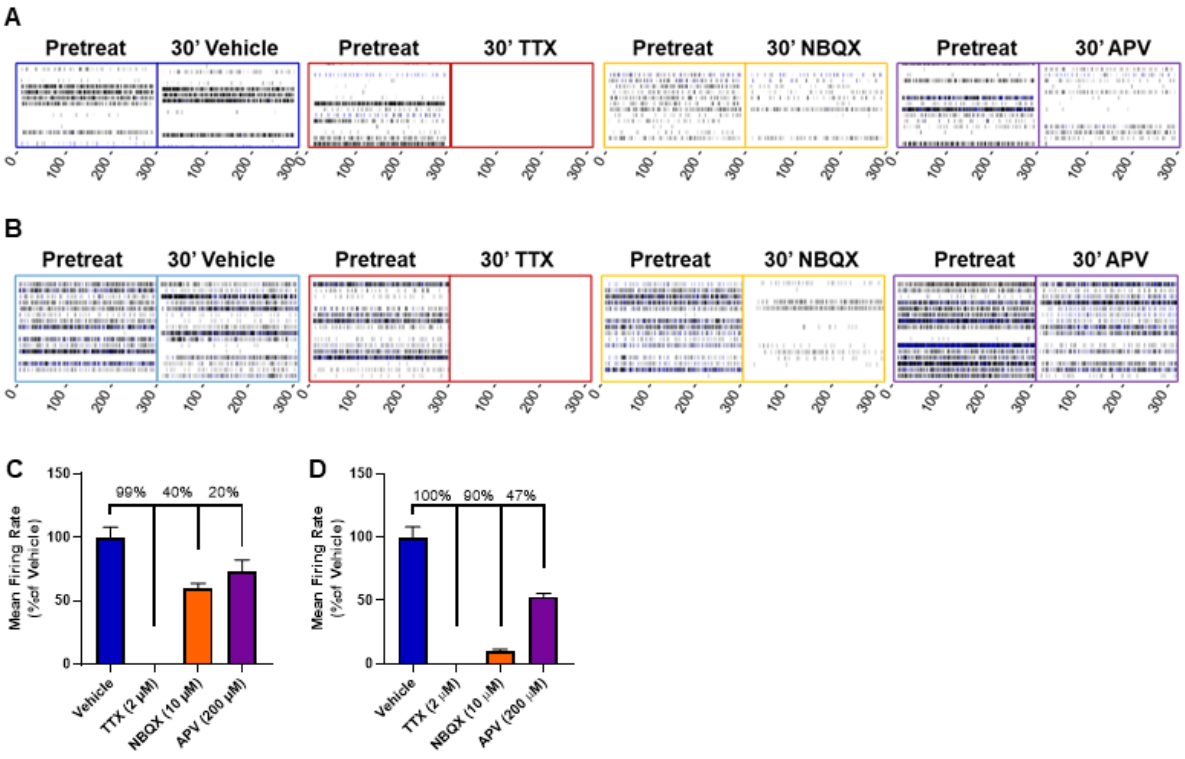

Supplemental Figure 3 – A) Representative Raster plots of 4WIV iEN before (pretreat) and 30" minutes after treatment with vehicle (0.1% DMSO), TTX (2 μM), NBQX (10 μM) or APV (200 μM, x axes = time in seconds, Y-axis rows indicate electrodes). B) Representative Raster plots of 7WIV iEN before (pretreat) and 30" minutes after treatment with Vehicle, TTX, NBQX or APV, as above. C) Quantification of 4WIV activity, percentage of baseline activity normalized to vehicle after treatment with the indicated inhibitors shown, with percentage inhibition indicated (n=10 wells per condition). D) Quantification of 7WIV activity, percentage of baseline activity normalized to vehicle after treatment with the indicated inhibitors shown, with percentage inhibition indicated (n=8 wells per condition).

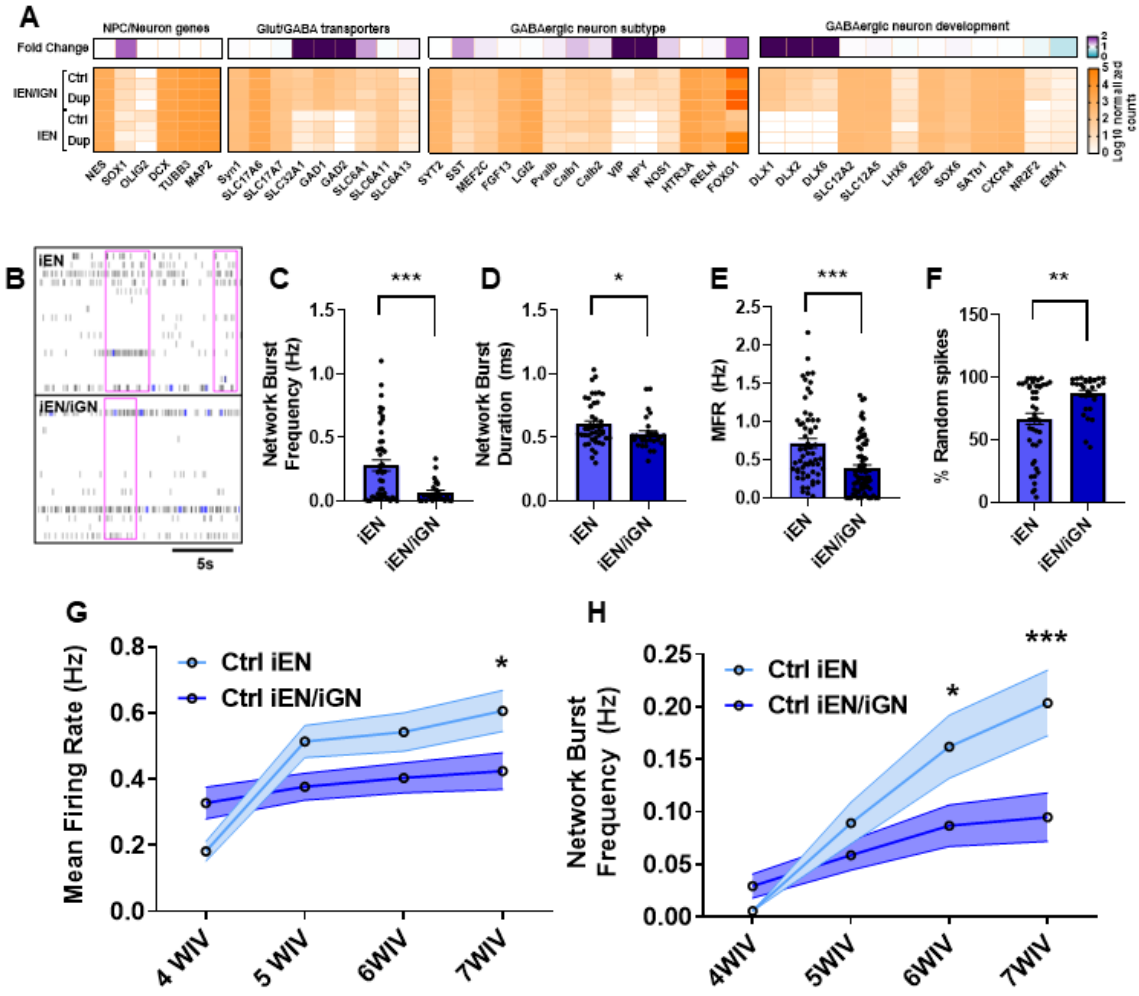

Supplemental Figure 4 - A) To confirm the integrity of iGNs within the coculture model, a transcriptomic profile of control and 16p11.2 duplication iENs and iEN/iGN coculture was generated (log normalized counts). Fold change between iENs and iENs/iGNs shown at top, where purple indicates >2 fold change in coculture to monoculture. Cocultured iENs/iGNs (80/20 ratio) showed increased expression of the GABAergic markers SLC32A1 (VGAT), GAD1, GAD2, SLC6A1 (GAT-1), SST, CALB1, NOS1, DLX1,2 and 6, as well as the telencephalon marker FOXG1, consistent with the presence of GABAergic neurons. B) Representative raster plot of iENs (top) and iENs/iGNs cocultures (bottom). Metrics altered by the presence of iGN; network burst frequency (C) and duration (D), mean firing rate (E) and % random spikes (F). In line with a previous report, the presence of iGNs resulted in a significant decrease in these metrics, consistent with iGN inhibitory activity (64). Developmental time course of mean firing rate (G) and network burst frequency (H) suggest iGN-induced developmental differences occur after 5WIV, consistent with reported time points relating to the GABA switch (the developmental period where GABAergic input switches from excitatory to inhibitory) in iPSC models (64). N=6, 2 clones per condition, 3 independent differentiations, n=48 wells per condition.

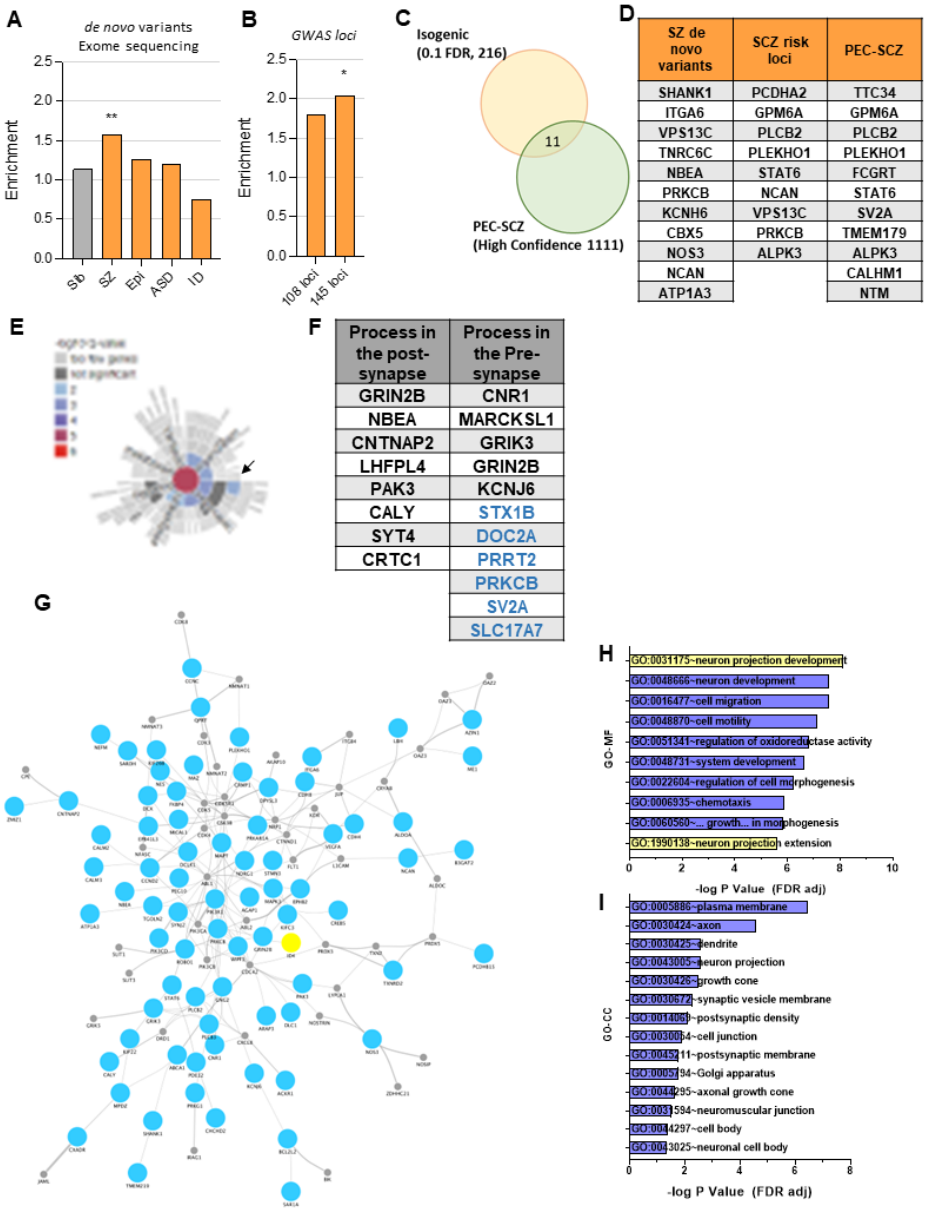

Supplemental Figure 5 – A) Enrichment of 16p11.2 duplication deregulated genes in SZ (Schizophrenia), EPI (epilepsy), ASD (autism spectrum disorder), ID (intellectual disability) and unaffected sibling controls (SIB) from *de novo* exome wide significant gene sets. B) Enrichment of SCZ GWAS loci in 16p11.2 duplication deregulated genesets. C) Overlap of Dup DEGs with the PsychENCODE high confidence SCZ gene set (63). d) Table of SCZ genes/loci identified in A-C. E) SynGO plot of compartments/processes affected by 16p11.2 duplication. Colored squares represent GO terms enriched in 16p11.2 duplication DEGs. Arrowhead indicates the significant third level term – "Synaptic vesicle release". F) Table of DEGs altered in the post and pre-synaptic compartments in DUP iEN. "Synaptic vesicle release" DEGs are highlighted in blue. G) Protein-protein interaction (PPI) network of dysregulated genes. H) GO-MF terms enriched within PPI network. I) GO-CC terms enriched within PPI network.

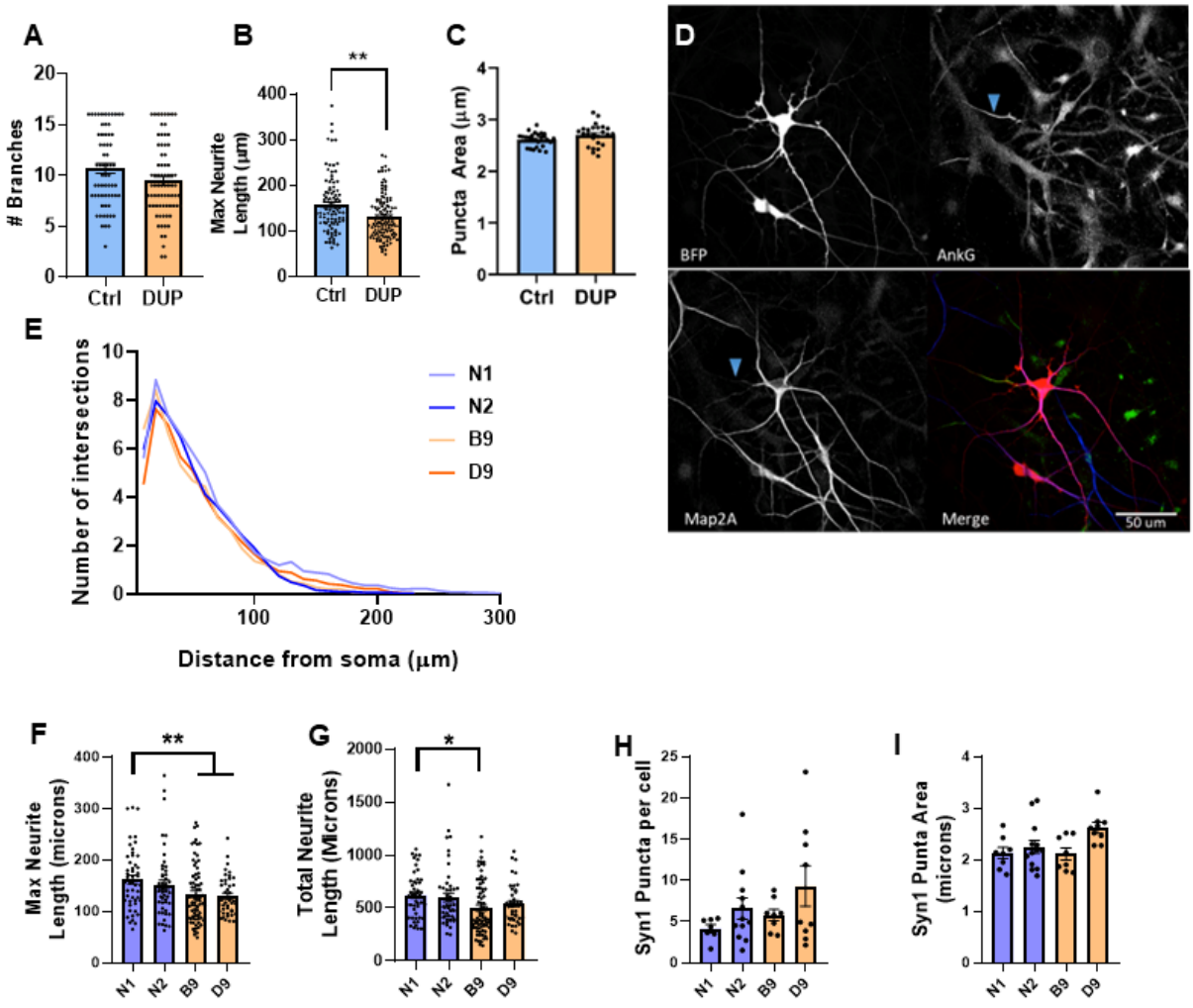

Supplemental Figure 6 – A) Branch point analysis of control (ctrl) and 16p11.2 duplication (DUP) iENs. B) Length of the longest neurite present in ctrl and DUP lines. C) Average size of Syn1 puncta. D) Representative image of control, BFP labeled iENs. The MAP2 negative, AnkyrinG (AnkG) positive axon initial segment is indicated (arrowhead) confirming MAP2 staining of dendrites only. Scale bar = 50 µM. E) clone by clone sholl analysis. F) Max neurite length of individual clones (N1/N2 = ctrl, B9/D9= DUP). G) Total neurite length of individual clones. H) Syn1 puncta density of individual clones. I) Syn1 puncta area of individual clones.

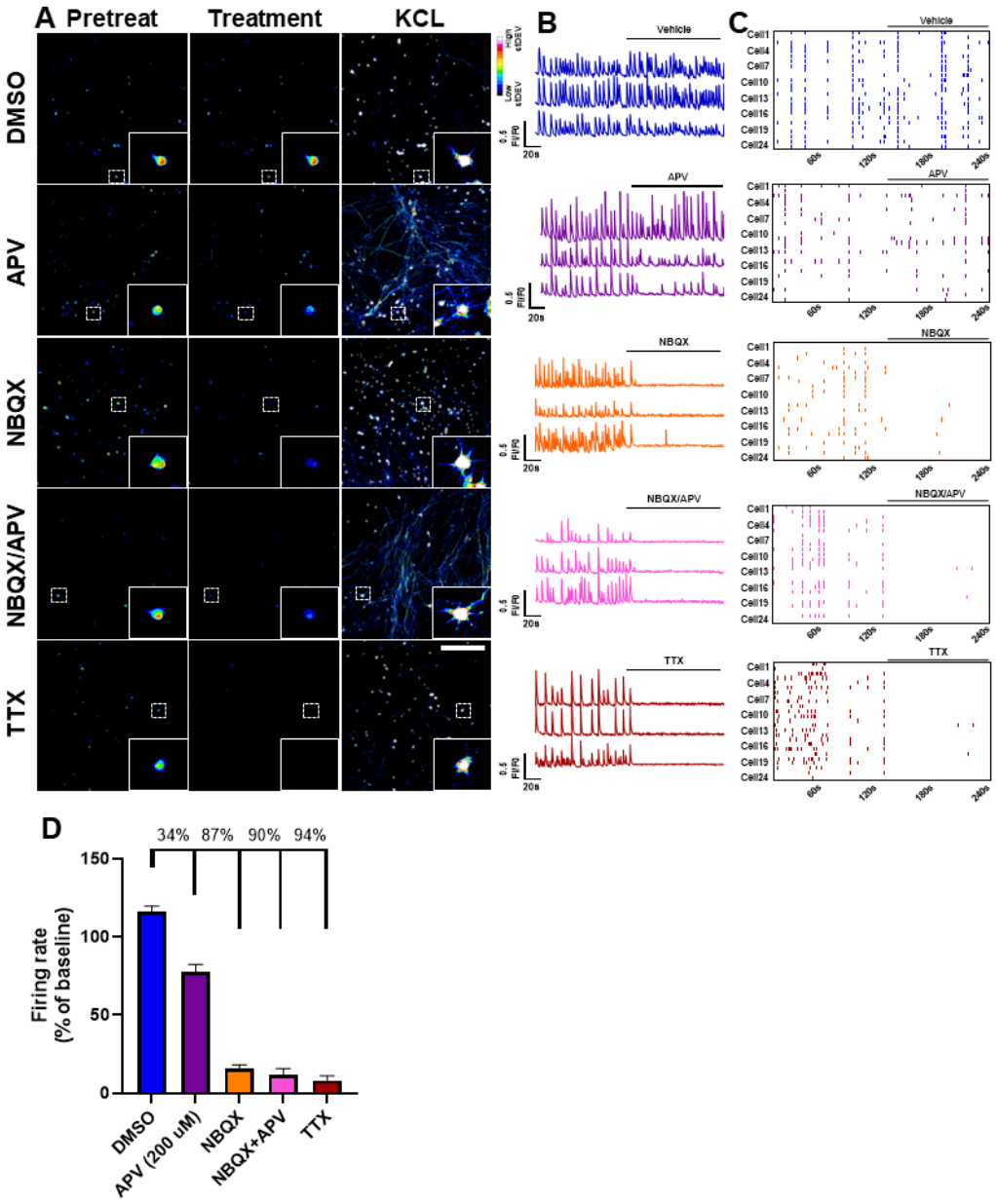

Supplemental Figure 7 – iPSC derived neurons were prepared for imaging as outlined for Fig 3,5. Baseline recordings were taken for 2 minutes (Pretreat), before bath application of the indicated treatments (Treatment, 2 mins). Cell viability was assessed after treatment by application of 30 mM KCL to induce depolarization of surviving neurons. A) standard deviation max projections showing the variation of signal over 2 minutes for each of the indicated treatment periods, and correlating to calcium events.B) ROIs were drawn over neurons and fluorescence intensity was measured at each time point before and after the indicated treatment (bar, 120s-240s). C) raster plot of 25 representative cells (rows) from each field of view, with events at each time point (columns) indicated by a line. D) quantification of compound effect (% of baseline activity, with % of vehicle indicated).

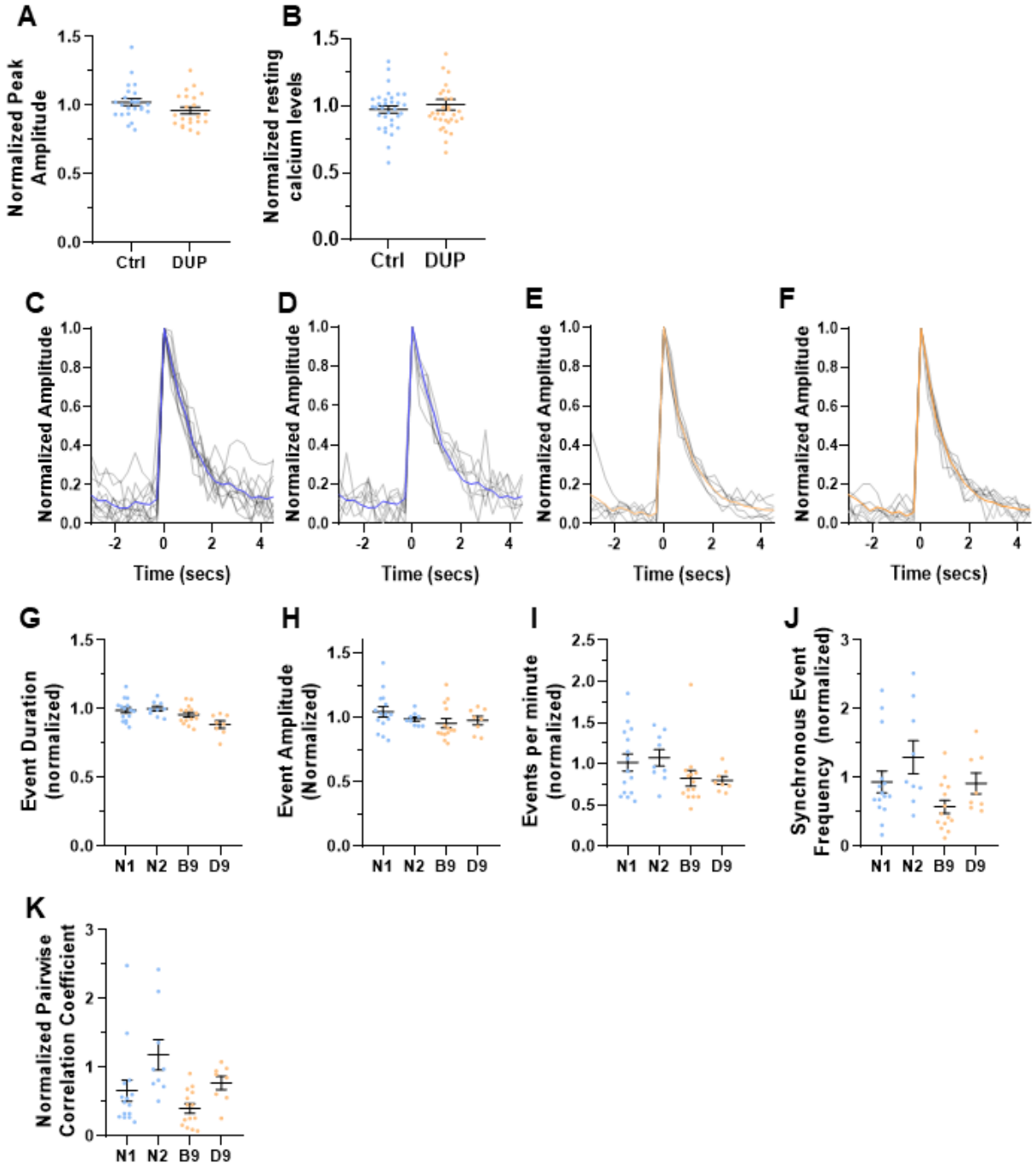

Supplemental Figure 8 – A) Calcium peak amplitude normalized within experiment to control. B) The mean calcium fluorescence intensity, normalized within experiment to control lines. Overlay of average control (clone N1 (C) and clone N2 (D)) and DUP (clone B9 (E) and clone D9 (F)) calcium peaks from control and 16p11.2 duplication neurons. Clone by clone calcium event duration (G), amplitude (H), frequency (I), synchronous event frequency (J) and pairwise correlation (K).

A

Patient ID	Designation	Age	Sex	Polygenic risk score (<0=increased risk, >0=decreased risk)	Clinical phenotype
02C12626	SCZ1	35	Male	-1.4404	Schizophrenia age at onset (AAO) 18 yo, with 22 years of active illness, and a positive family history of schizophrenia; also with attention deficit hyperactivity disorder (ADHD) diagnosis since grade school. Completed 12th grade. Medical history also includes seizure disorder since 5 yo, and being a daily smoker (4 cigarettes per day, CPD).
04C27671	SCZ2	34	Female	-0.344853	Schizoaffective disorder (manic type) AAO 15 yo, with 19 years of active illness. Completed a Bachelor's degree. Medical history includes irritable bowel syndrome and seizures.
06C58821	SCZ3	38	Male	-1.28264	Schizophrenia AAO 22 yo, with 16 years of active illness; also had depressive disorder NOS (not otherwise specified) and was diagnosed with ADHD as a youth. Completed 12th grade, and later some job corps training. Medical history includes febrile seizures as a child, and being a daily smoker (40 CPD).
06C52982	Healthy1	38	Male	0.666804	Completed a Bachelor's degree.
05C51897	Healthy2	35	Male	-1.16313	Completed a Bachelor's degree. Daily smoker (10 CPD).
05C44627	Healthy3	34	Male	NC (Insufficient imputations)	Completed a Master's degree.

B

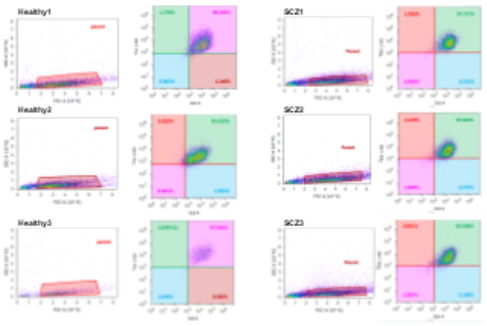

C

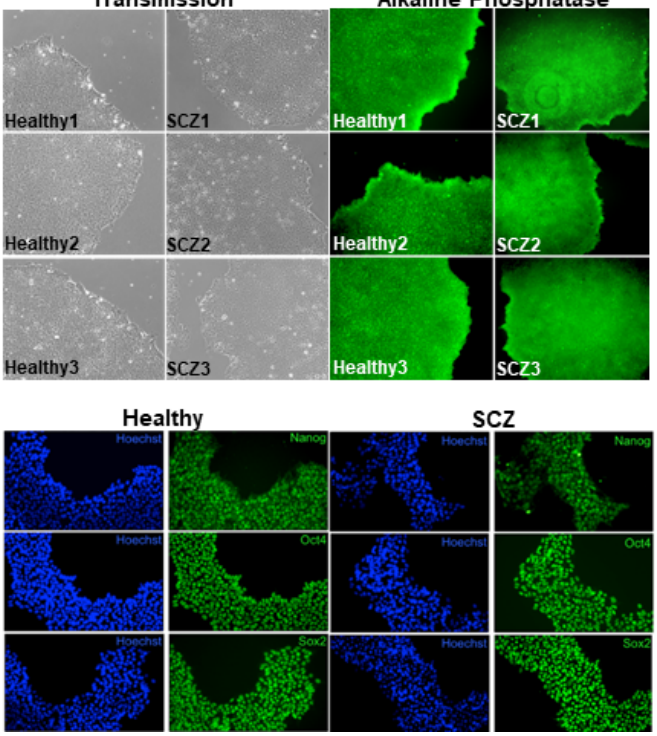

D

Dup1

Chr	CNV value	Start	End	Size (Mbp)	CNV confidence (35 = minimum)	Comments
10	3	135,256,762	135,378,802	0.12204	497.00	
13	3	21,728,134	21,732,094	0.00396	51.44	
16	3	29,595,483	30,215,621	0.62014	538.72	
2	1	242,918,203	243,034,519	0.11632	37.58	
7	0	38,297,145	38,367,259	0.07011	2291.70	TCRGC2
7	1	141,581,325	142,196,434	0.61511	305.54	TCRVB
24	0	22,434,423	22,988,571	0.55415	17313.91	TCRa
24	1	22,338,459	22,433,866	0.09541	89.29	TCRa

DUP2

Chr	CNV value	Start	End	Size (Mbp)	CNV confidence (35 = minimum)	Comments
1	3	1,138,913	1,366,830	0.22792	49.75	
6	3	168,336,080	168,597,552	0.26147	815.28	
15	3	25,414,437	25,480,960	0.06652	38.60	
16	3	29,595,483	30,400,307	0.80482	391.36	
16	3	75,532,044	75,593,083	0.06104	205.84	
17	3	44,169,808	44,580,136	0.41033	67.28	
20	3	29,805,100	30,621,098	0.81600	729.05	Known iPSC CNV
6	1	67,017,494	67,047,294	0.02980	56.82	
10	1	58,904,859	58,937,708	0.03285	56.04	
7	0	38,319,339	38,335,520	0.01618	722.50	TCRGC2
7	0	142,330,328	142,493,129	0.16280	1589.67	TCRVB
7	1	142,022,250	142,328,771	0.30652	37.85	TCRVB
14	0	22,477,415	22,984,586	0.50717	17709.01	TCRa
14	1	22,221,211	22,471,333	0.25012	312.63	TCRa

DUP3

Chr	CNV value	Start	End	Size (Mbp)	CNV confidence (35 = minimum)	Comments
16	3	29,595,483	30,215,621	0.62014	136.84	
17	3	5,577,442	5,722,564	0.14512	264.37	
19	3	57,483,008	57,661,622	0.17861	191.52	
3	0	75,428,675	75,636,449	0.20777	467.94	
14	0	22,362,142	22,985,006	0.62286	21300.41	TCRa
7	0	38,297,145	38,385,938	0.08879	2831.39	TCRGC2
7	1	142,030,318	142,493,129	0.46281	74.15	TCRVB
14	1	22,221,211	22,356,225	0.13501	103.57	TCRa

Supplemental Figure 9 – A) Schizophrenia patient & controls clinical information, polygenic risk and identifiers. Patient IDs refer to phs000021.v2.p1 and phs000167.v1.p1 (65-67). Controls were negative on screening questions for schizophrenia (diagnosis, treatment, symptoms), and also had no common psychiatric diagnoses present as assessed by composite international diagnostic interview – short form (i.e., negative for depression, generalized anxiety disorder, specific phobia, social phobia, agoraphobia, panic attacks, obsessive compulsive disorder, alcohol dependence, drug dependence). All subjects self-identified as European ancestry. Controls were not assessed for medical disorders. B) FACs analysis following derivation to confirm stem cell state after reprogramming. C) Representative images of healthy and SCZ 16p11.2 patient iPSCs with transmission images of colonies, alkaline phosphatase uptake and stained with indicated stem cell markers. D) CNV analysis of SCZ lines indicating the size and positions of 16p11.2 duplication.

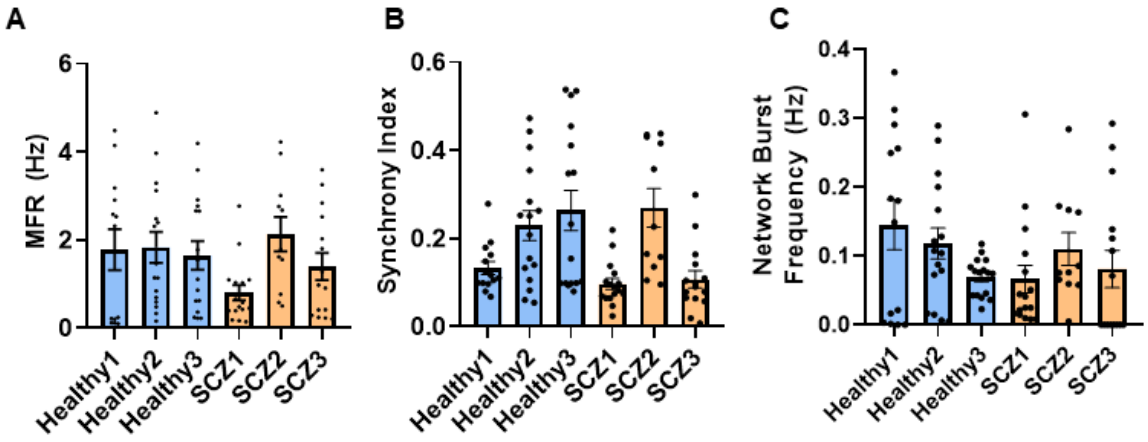

Supplemental Figure 10 – Patient by patient MEA assessment of mean firing rate (A), synchrony index (B) and network burst frequency (C).

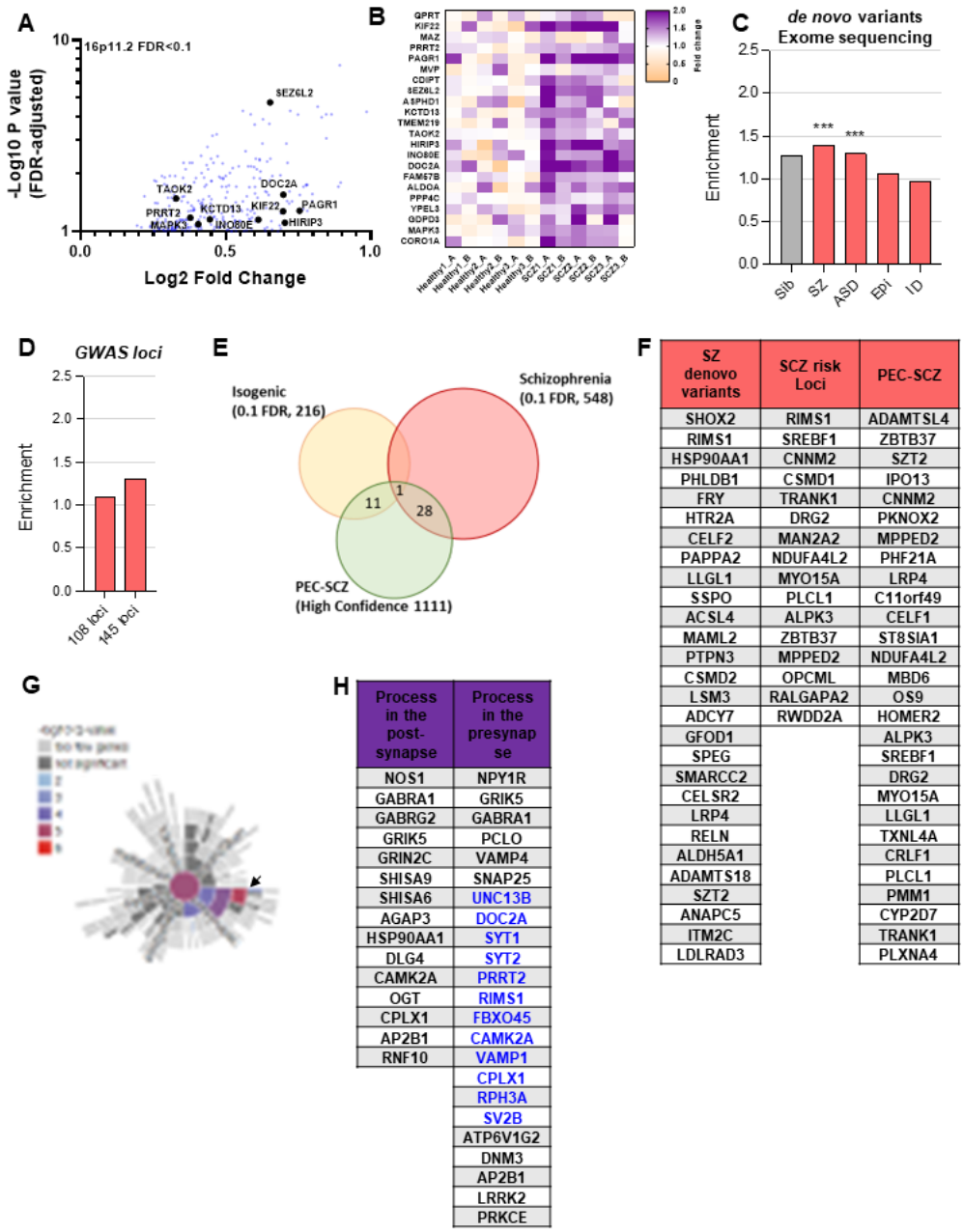

SZ denovo variants	SCZ risk Loci	PEC-SCZ
SHOX2	RIMS1	ADAMTSL4
RIMS1	SREBF1	ZBTB37
HSP90AA1	CNNM2	SZT2
PHLDB1	CSMD1	IPO13
FRY	TRANK1	CNNM2
HTR2A	DRG2	PKNOX2
CELF2	MAN2A2	MPPED2
PAPPA2	NDUFA4L2	PHF21A
LLGL1	MYO15A	LRP4
SSPO	PLCL1	C11orf49
ACSL4	ALPK3	CELF1
MAML2	ZBTB37	ST8SIA1
PTPN3	MPPED2	NDUFA4L2
CSMD2	OPCML	MBD6
LSM3	RALGAPA2	OS9
ADCY7	RWDD2A	HOMER2
GFOD1		ALPK3
SPEG		SREBF1
SMARCC2		DRG2
CELSR2		MYO15A
LRP4		LLGL1
RELN		TXNL4A
ALDH5A1		CRLF1
ADAMTS18		PLCL1
SZT2		PMM1
ANAPC5		CYP2D7
ITM2C		TRANK1
LDLRAD3		PLXNA4

Process in the post-synapse	Process in the presynapse
NOS1	NPY1R
GABRA1	GRIK5
GABRG2	GABRA1
GRIK5	PCLO
GRIN2C	VAMP4
SHISA9	SNAP25
SHISA6	UNC13B
AGAP3	DOC2A
HSP90AA1	SYT1
DLG4	SYT2
CAMK2A	PRRT2
OGT	RIMS1
CPLX1	FBXO45
AP2B1	CAMK2A
RNF10	VAMP1
	CPLX1
	RPH3A
	SV2B
	ATP6V1G2
	DNM3
	AP2B1
	LRRK2
	PRKCE

Supplemental Figure 11 – A) Volcano plot indicating 16p11.2 genes upregulated in SCZ patients (FDR<0.1). B) Heat plot of all expressed 16p11.2 genes. C) Enrichment of SCZ patient lines' deregulated genes in SZ (Schizophrenia), EPI (epilepsy), ASD (autism spectrum disorder), ID (intellectual disability) and unaffected sibling controls (SIB) *de novo* exome wide significant gene sets. D) Enrichment of SCZ patient lines' deregulated genes in reported SCZ GWAS loci. The absence of SCZ risk loci enrichment suggest that outside of the 16p11.2 duplication each of the 3 SCZ lines do not share common SCZ risk markers. E) overlap between isogenic lines, patient lines and the PsychENCODE high confidence SCZ gene set. F) DEGs arising from C-F. G) A synaptic GO ontology map was generated for SCZ 16p11.2 duplication lines. Colored squares represent GO terms enriched in 16p11.2 duplication deregulated mRNAs. Arrowhead indicates the significant third level term – "Synaptic vesicle release". H) Table of DEGs altered in the post and pre-synaptic compartments in DUP iEN. "Synaptic vesicle release" DEGs are highlighted in blue.

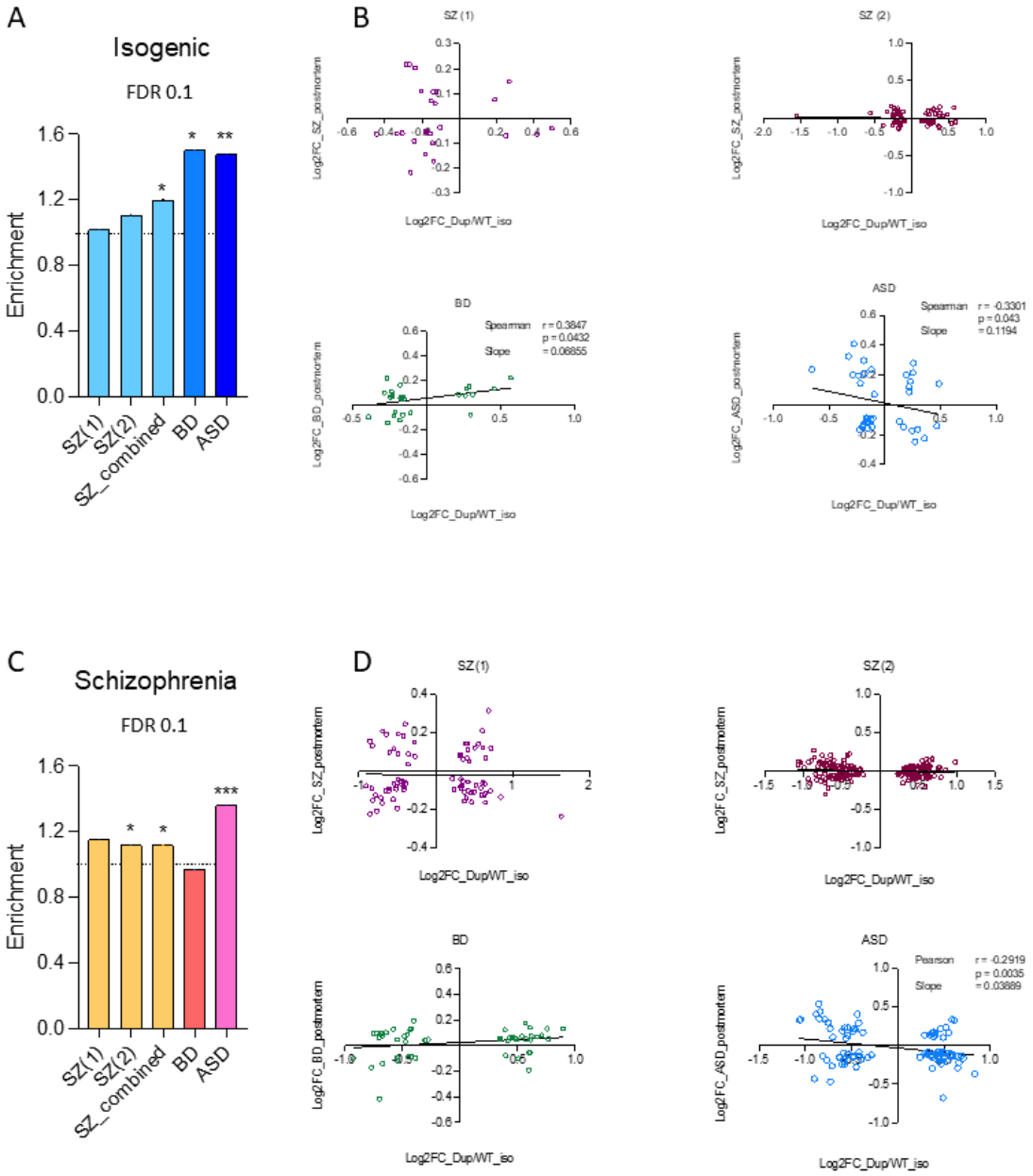

Supplemental Figure 12 – Enrichment of transcriptional changes from iEN in post-mortem brain samples associated with psychiatric disorders (PsychENCODE Consortium (63)). Gene sets of differentially expressed genes in isogenic (A) and patient (B) stem cell derived neurons (FDR<0.1) were overlapped with gene sets from transcriptome dysregulation in psychiatric disorders. Gene set enrichment analysis revealed enrichment across various disorders in both isogenic and patient data sets. The SZ(1) dataset was obtained from (68), whilst SZ(2), BD and ASD were from (69). SZ_combined includes both SZ(1) and SZ(2) data. Results from a hypergeometric test are displayed on the bar graphs with *, P<0.05; **, P<0.01; ***, P<0.001. Correlation analysis between post mortem RNA-seq in psychiatric disorders and RNA-seq data from (B) isogenic lines or (D) SCZ patient lines. Correlation plots show fold changes of genes affected in both studies. The correlation coefficient (Pearson's for parametric data and Spearman's for non-parametric data) and associated p-value as well as the slope of the linear regression are indicated on graphs where a significant correlation was found.

A

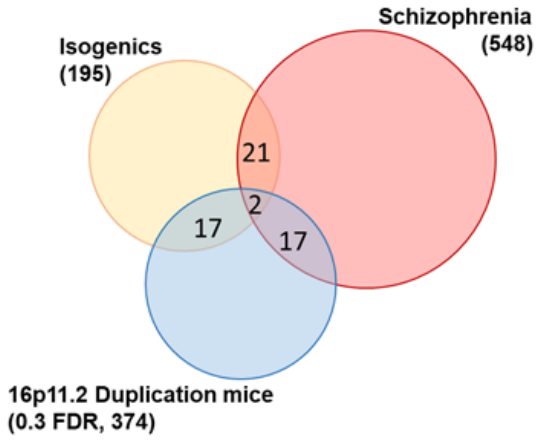

B

Isogenic (excluding 16P)	Patient (excluding 16P)	Isogenic / Patient
BNC2	ST8SIA1	INF2
SHANK1	XYLT1	ASXL3
PCDHB2	SHISA6	
GDPD3	ZFHX2	
GRIN2B	CELF2	
RNF152	PAPPA2	
WIPF3	POU2F2	
ASXL3	SRRM4	
GRIK3	VWA7	
INF2	PCDHA11	
ACKR1	SSPO	
ZMIZ1	ZFPM2	
DCX	INF2	
TENM2	ASXL3	
ATP1A3	NOS1	
SEMA5A	CSMD2	
PRRC2B	TCP11L1	

C

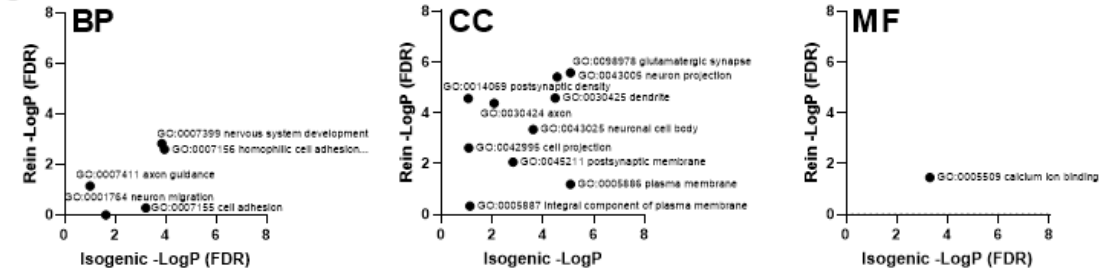

Supplemental Figure 13 – A) overlap in DEGs from isogenic and SCZ lines with 16p11.2 duplication mouse cortex (7). B) table of overlapping DEGs identified in (A). C) GO terms shared between isogenic, patient and mouse cortex data sets.

A

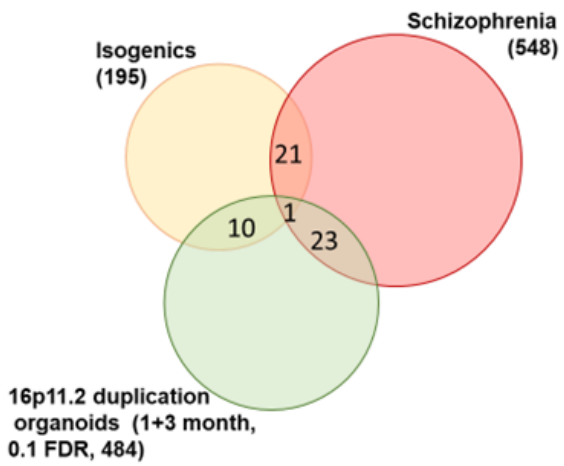

B

Isogenic (excluding 16P)	Patient (excluding 16P)	Isogenic / Patient
LMO3	ACSL3	GFR1A
CXADR	THAP9-AS1	
CALM3	GFRA1	
RNF152	DLG4	
GFRA1	DRAXIN	
UBE2QL1	TRIM36	
GNPTAB	CELF2	
DTX4	CDH18	
AKNA	TIMM50	
	NR2F1	
	ATP6V1G2	
	RALGAPA2	
	SNHG7	
	RPL10A	
	PCK2	
	UNC13B	
	TOMM20	
	BAZ1A	
	SLC16A14	
	TMBIM4	
	MAGI2-AS3	
	KIAA1024	
	GTF2H5	

C

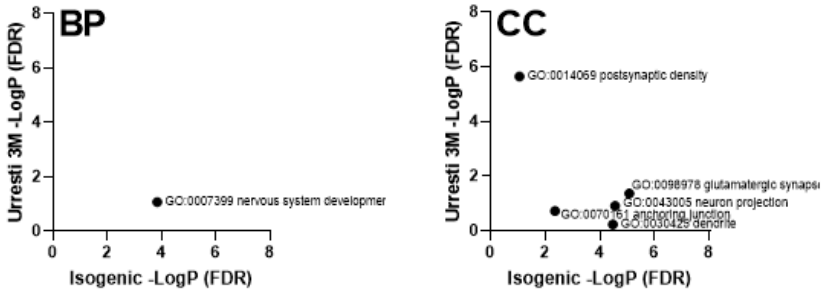

Supplemental Figure 14 – A) overlap in DEGs from isogenic and SCZ lines with 16p11.2 duplication cortical organoids (DEGs compiled from 1M and 3M data sets (18)). B) table of overlapping DEGs identified in (A). C) GO terms shared between isogenic, SCZ and 16p11.2 duplication organoid data sets.

A

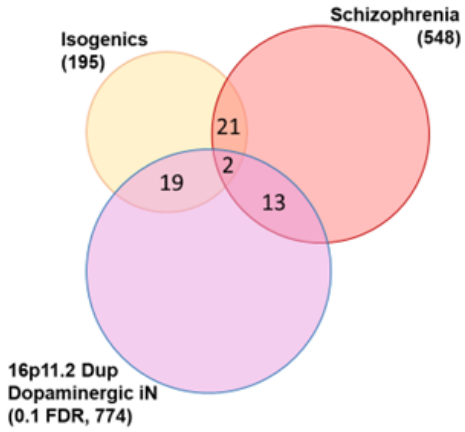

B

Isogenic (excluding 16P)	Patient (excluding 16P)	Isogenic / Patient
ZNF736	SLC1A3	KIDINS220
SYT4	SLITRK2	ONECUT1
PCDHB5	MIR9-3HG	
LMO3	ADAMTS18	
EFR3B	ACSL3	
B3GAT2	KIDINS220	
GNG2	CD27-AS1	
EBF3	CSMD3	
RAB3C	ONECUT1	
ONECUT2	STK32A	
ONECUT1	GPCPD1	
HPCAL1	CDH12	
RNF152	RUNX1T1	
CDH8	RELN	
GRIK3	KLHL2	
PRKCB	ZC3H15	
KIDINS220	SLC16A14	
SVOP		
GARNL3		

C

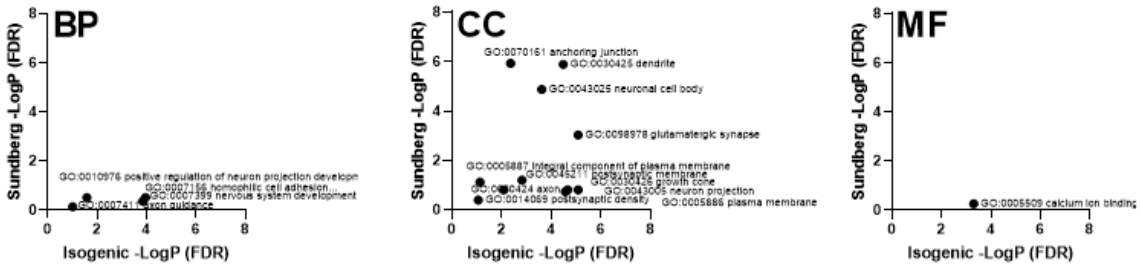

Supplemental Figure 15 – A) Overlap in DEGs from isogenic and SCZ lines with 16p11.2 duplication isogenic iPSC- (70) derived dopaminergic neurons (19). B) table of overlapping DEGs identified in (A). C) GO terms shared between isogenic, SCZ and 16p11.2 duplication dopaminergic iN data sets.

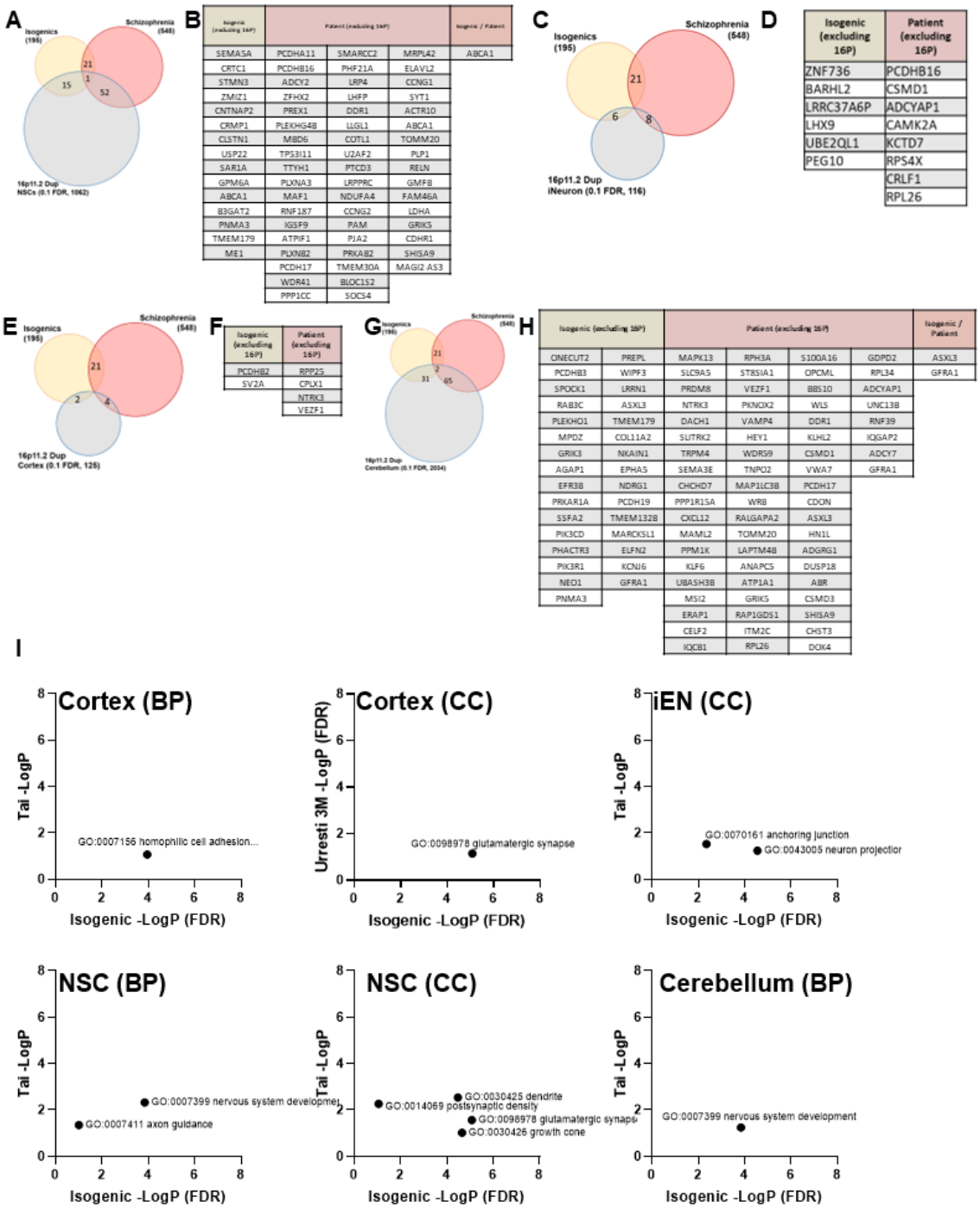

Supplemental Figure 16 – Venn diagram and table of overlapping DEGs from isogenic and SCZ lines with 16p11.2 duplication isogenic (70) iPSC-derived neural stem cells (NSC, A,B), iEN (C,D), and mouse cortex (E,F) and cerebellum (G,H) RNA-seq data sets (8). Note, no overlapping DEGs were found within mouse striatum (data not shown). I) GO terms shared between isogenic, SCZ and 16p11.2 duplication dopaminergic iPSC NSC, iEN and mouse cortex, cerebellum data sets (tables omitted for GO categories/tissues with no overlap).

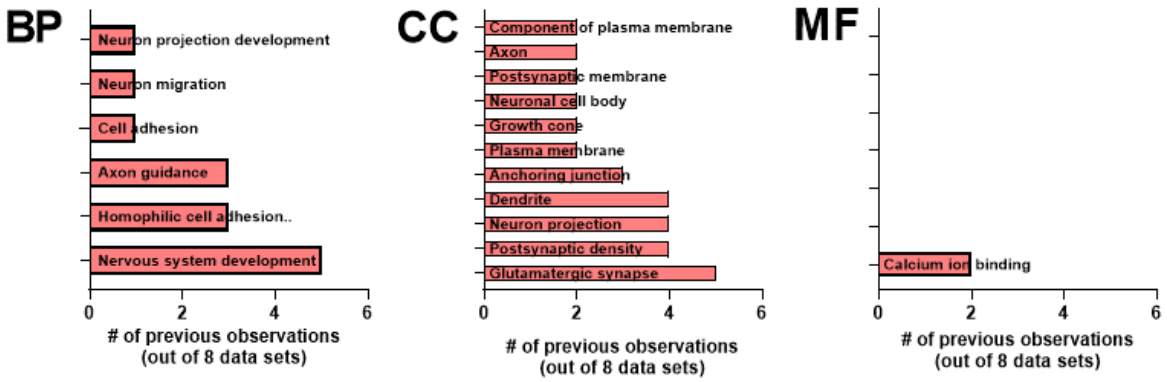

Supplemental Figure 17 – GO terms identified within this study, observed in previous RNA-seq data sets (Fig S13-S16). Note, “Nervous system development”, “Neuron projection”, “Neuron projection development”, “Axon” and “Cell projection” and altered protocadherin family gene expression were also reported in (71).

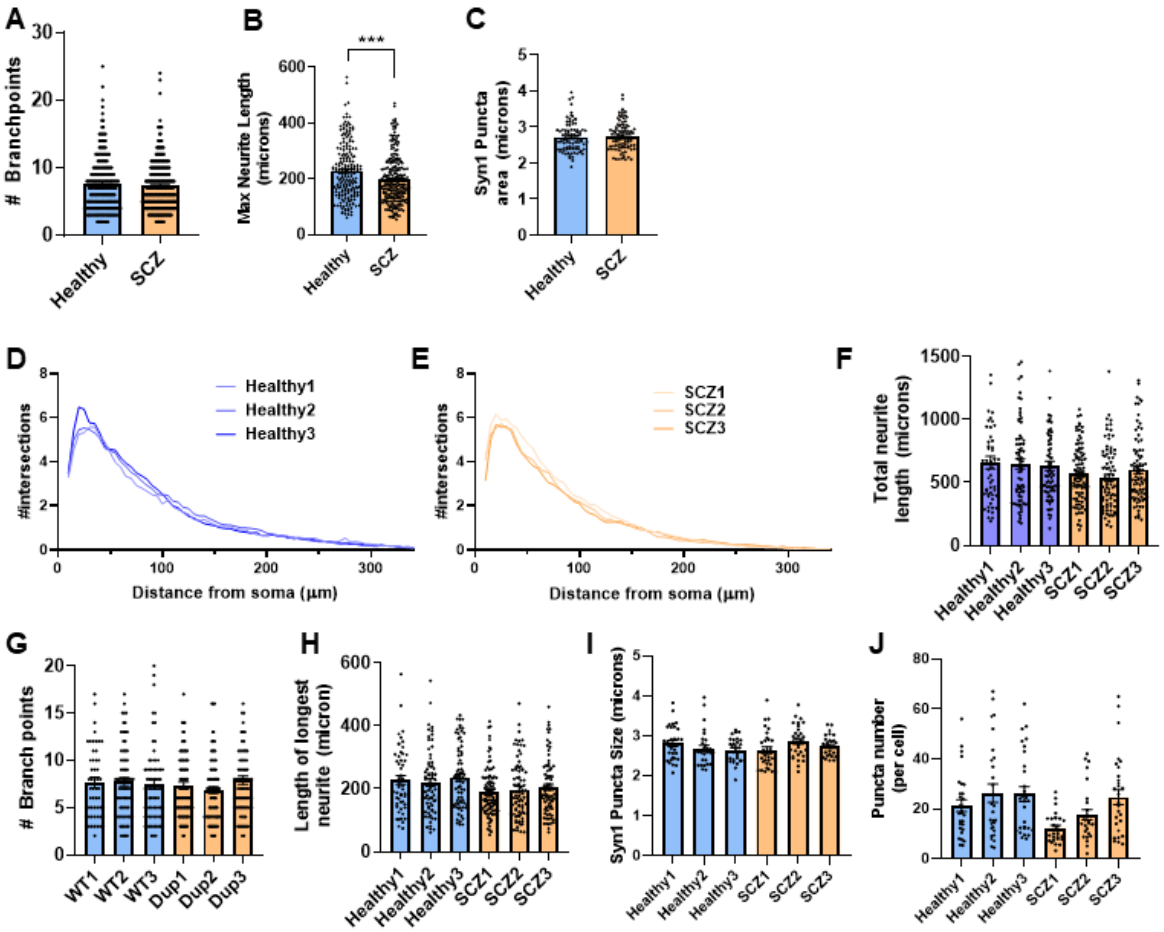

Supplemental Figure 18 – A) Branch point analysis of healthy and SCZ iENs B) Length of the longest neurite present in healthy and SCZ lines. C) Syn1 puncta size. D-E) Patient by patient sholl analysis. F) Patient by patient neurite outgrowth. G) Patient by patient branchpoint analysis. H) Patient by patient length of longest neurite. I) Patient by patient Syn1 puncta size. J) Patient by patient Syn1 puncta per line.

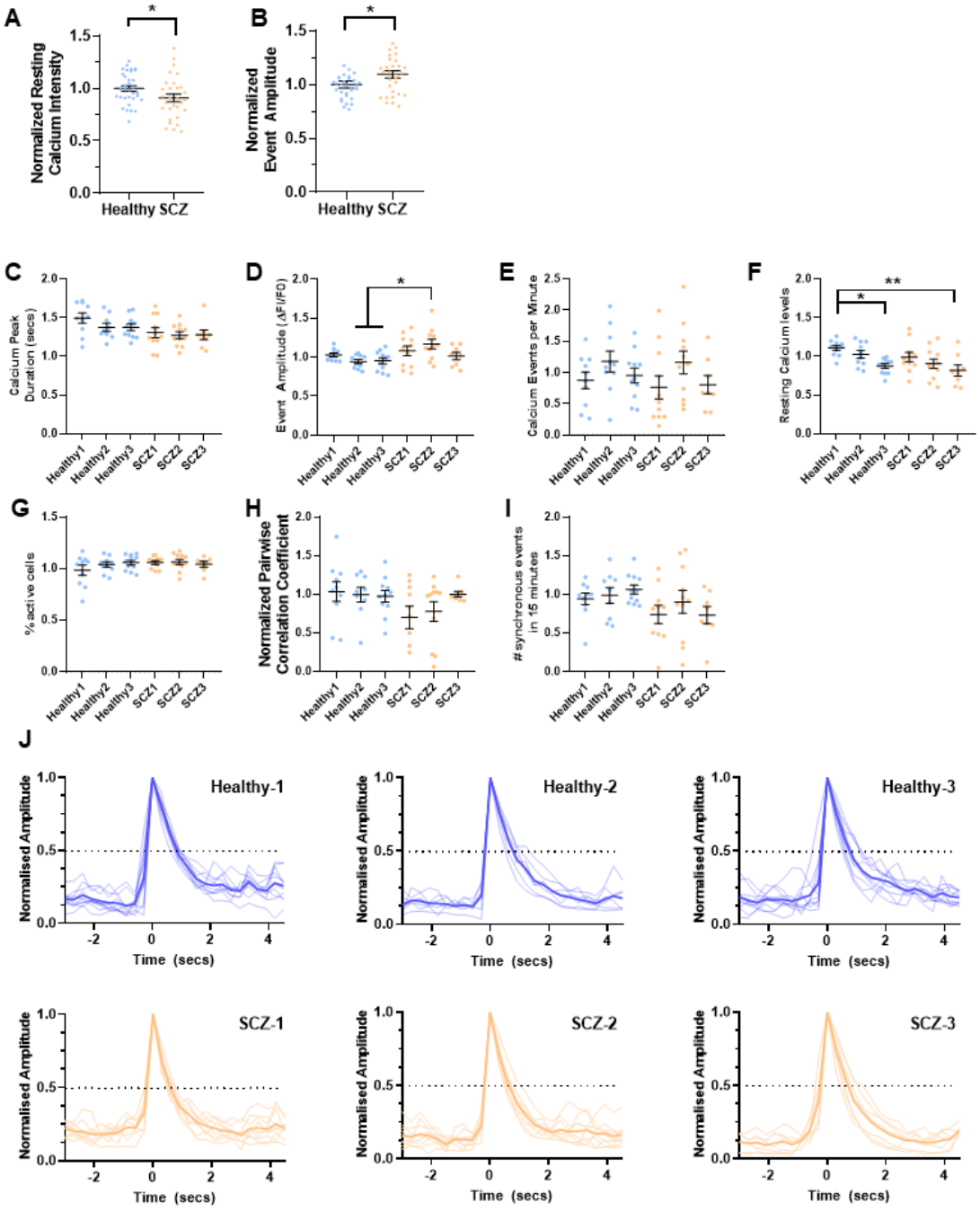

Supplemental Figure 19 – A) Resting calcium fluorescence of iENs normalized within experiment to healthy lines. B) Event amplitude normalized within experiment to healthy lines. C) Calcium event duration of each individual patient line. D) Calcium event amplitude of each individual patient line. E) Calcium event frequency of each individual patient line. F) Resting calcium levels of each individual patient line. G) % of active cells of each individual patient line. H) Pairwise correlation of each individual patient line. I) Synchronous firing of each individual patient line. J) Calcium peak overlay from individual patients. Average peak trace of 10 individual events from 10 cells per line.

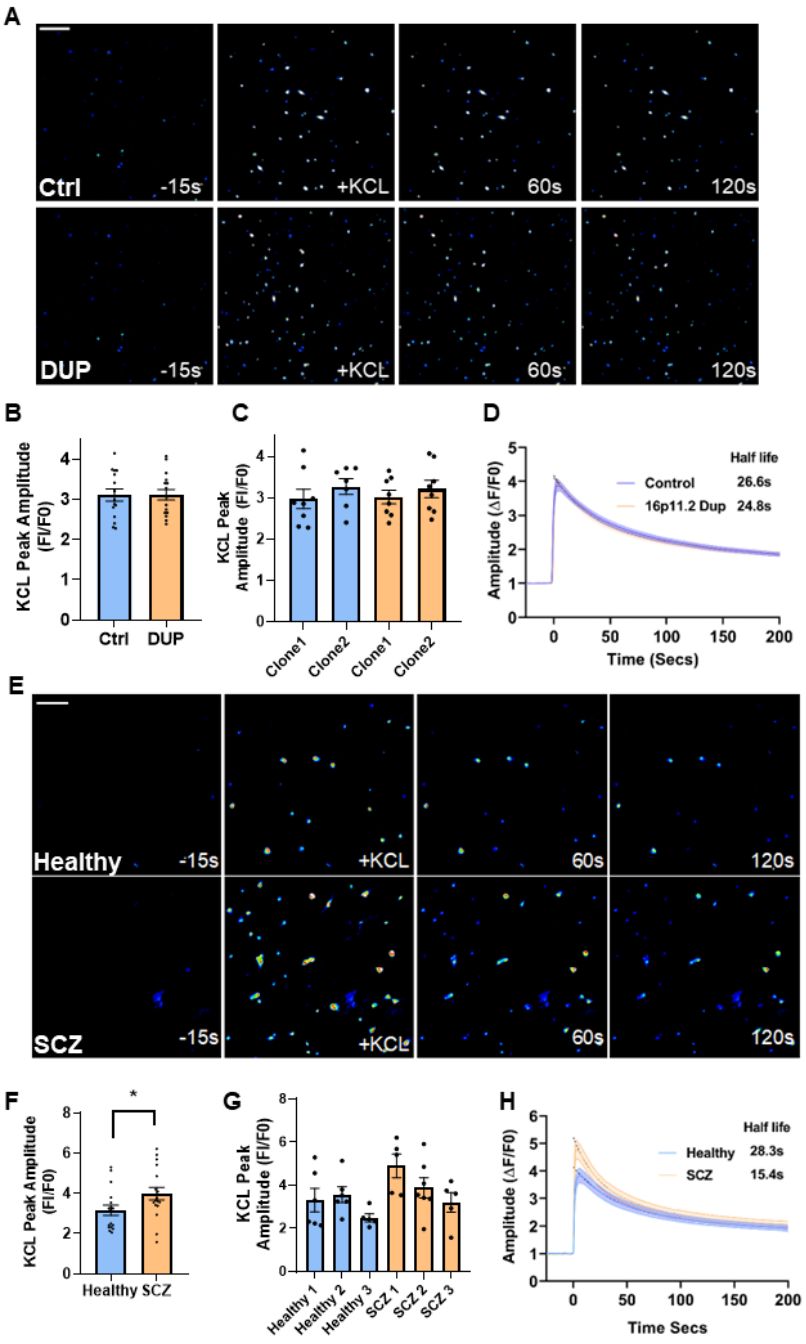

Supplemental Figure 20 – A) Representative field of view of isogenic control (Ctrl) and 16p11.2 duplication (DUP) iENs prior to and following KCl (30 mM) induced depolarization at given time points. B) KCl induced calcium peak amplitude (fold change over baseline). C) Clone by clone event amplitude. D) Recovery following KCl depolarization was plotted and fitted with a two-phase exponential decay to identify decay rate (half-life indicated). E) Representative field of view of healthy and SCZ iENs. Calcium intensity was measured prior to and following KCl (30 mM) induced depolarization. F) KCl induced calcium peak amplitude (fold change over baseline). G) line by line depolarization induced amplude. H) Recovery following KCl depolarization was plotted and fitted with a two-phase exponential decay to identify decay rate (half-life indicated).

Ref (Supplemental)	Differentiation protocol / cell type / Age	Phenotypes observed	Comparison / contrast
(19)	Dopaminergic iEN employing isogenic lines (70) derived from a male patient, 27-60DIV	• Unchanged Spontaneous/evoked firing (60DIV) • Unchanged activity/synchrony (27-60DIV) • Reduced synaptic puncta (SYN1/PSD95) (60DIV) • Reduced SYP1 puncta (60DIV)	• Inconsistent results may be due to different cell type (iEN vs dopaminergic), level of maturity, network development (although up to 60DIV, cultures are on MEAs for only 28DIV). • PSD95/Syn1 overlap may account for altered synaptic puncta density.
(18)	Cortical Organoids (72), 3x 16p11.2 duplication male carriers, selected based on head circumference with varying diagnoses (1xASD+ID, 1xID, 1xADHD), 1 + 3MIV	• Decreased organoid size • No neurite outgrowth deficits (trending) • Syn1 puncta unchanged • Cell migration reduced • Increased active RhoA expression	• Neuron, Age or altered differentiation method may account for disparity in neurite outgrowth • Notably this is the only previous study to assess Syn1 alone, and also observes no alteration in density
(8)	iEN (73), 25DIV, Organoids (74), 6MIV, Isogenic lines (70) derived from a male patient	• Decreased neurite length (iEN, 0, 4, 8DIV) • Decreased branching (iEN, 0,4,8DIV) • Decreased activity (DIV25) • Decreased Synchrony (DIV25) • Decreased oscillation (DIV25) • Altered excitatory/inhibitory ratio (6MIV)	• High convergence of MEA phenotypes lines/differentiation protocol, cross-corroborating our results with regards to activity / synchrony / neurite length • Altered age of phenotypic presentation (1WIV earlier) may account for plating differences (higher density may promote network development).
(17)	iEN (75), 2 male / 1 female, 16p11.2 duplication carriers (1x ASD, 1x microcephaly, 1x no diagnosis), 60-100DIV	• Increased mEPSC amplitude (~100DIV) • Unchanged spontaneous/evoked AP • Reduced Synaptic density (Syn1/Homer and Vglut/PSD95, 60DIV) • Reduced dendrite length (60DIV) • Unchanged branching (60DIV) • Decreased soma size	• Differences may be accounted for by data acquisition and differentiation methods. The presence of a 16p11.2 female line may complicate phenotypic presentation • Synaptic puncta density may be due to pre/post dual staining, as for (49)
This study	iEN (73), iGN (6). Isogenic lines (70) derived from a male patient. 3x SCZ patient lines (2 male+1Female)	• Decreased activity (isogenic, variable in patient lines) • Decreased synchrony (isogenic+patient) • Altered calcium homeostasis (isogenic+patient) • Reduced dendrite length (isogenic + patient) • SYN1 puncta number size unaltered (isogenic), reduced (patient)	• Matches (8) • Matches (8) • Novel finding • Observed in (17, 8) • Unaltered previously observed (18), (pre+post synapse staining reveals deficits (17, 19)

Supplemental Figure 21 – Summary of identified iEN phenotypes with comparison to recent iPSC derived 16p11.2 duplication studies.

Supplemental Table Legends

Supplemental Table 1 – Significant DEGs (Isogenic 16p11.2 duplication). Transcriptomic analyses yielded 216 genes with significantly altered expression (FDR<0.1).

Supplemental Table 2 – GO analyses (isogenic). Significantly altered genes were submitted to DAVID, using all expressed genes (>5 read counts) as a background. Shown are the background gene set, and GO results grouped into up and down regulated terms, with sub-ontologies molecular function, cellular component and biological process.

Supplemental Table 3 - SynGO Analyses (isogenic). All DEGs were submitted to SynGo, using expressed genes (>5 read counts) as a background (See Table S2).

Supplemental Table 4 - Protein-Protein interaction GO analyses (isogenic). Isogenic PPI network was assessed using DAVID to identify network dysfunction based on predicted expressed PPI networks.

Supplemental Table 5 – Significant DEGs (SCZ patient with 16p11.2 duplication). Transcriptomic analyses yielded 558 genes with significantly altered expression (FDR<0.1).

Supplemental Table 6 - GO analyses (Patient). Significantly altered genes were submitted to DAVID, using all expressed genes (>5 read counts) as a background. Shown are the results, grouped into up and downregulated terms in sub-ontologies molecular function, cellular component and biological process.

Supplemental Table 7 - SynGO Analyses (Patient). Significantly altered genes were submitted to SynGo, using all expressed genes (>5 read counts) as a background (See Table S7).

Supplemental Table 8 – Antibodies employed with vendors.

Supplemental References

1. Skene NG, Bryois J, Bakken TE, Breen G, Crowley JJ, Gaspar HA, et al. (2018): Genetic identification of brain cell types underlying schizophrenia. *Nat Genet*. 50:825-833.
2. Lewis DA, Curley AA, Glausier JR, Volk DW (2012): Cortical parvalbumin interneurons and cognitive dysfunction in schizophrenia. *Trends Neurosci*. 35:57-67.
3. Uhlhaas PJ, Singer W (2010): Abnormal neural oscillations and synchrony in schizophrenia. *Nat Rev Neurosci*. 11:100-113.
4. Grent-'t-Jong T, Gross J, Goense J, Wibral M, Gajwani R, Gumley AI, et al. (2018): Resting-state gamma-band power alterations in schizophrenia reveal E/I-balance abnormalities across illness-stages. *Elife*. 7.
5. Ahnaou A, Huysmans H, Van de Casteele T, Drinkenburg W (2017): Cortical high gamma network oscillations and connectivity: a translational index for antipsychotics to normalize aberrant neurophysiological activity. *Transl Psychiatry*. 7:1285.
6. Li S, Hu N, Zhang W, Tao B, Dai J, Gong Y, et al. (2019): Dysconnectivity of Multiple Brain Networks in Schizophrenia: A Meta-Analysis of Resting-State Functional Connectivity. *Front Psychiatry*. 10:482.
7. Rein B, Tan T, Yang F, Wang W, Williams J, Zhang F, et al. (2020): Reversal of synaptic and behavioral deficits in a 16p11.2 duplication mouse model via restoration of the GABA synapse regulator Npas4. *Mol Psychiatry*.
8. Tai DJC, Razaz P, Erdin S, Gao D, Wang J, Nuttle X, et al. (2022): Tissue- and cell-type-specific molecular and functional signatures of 16p11.2 reciprocal genomic disorder across mouse brain and human neuronal models. *Am J Hum Genet*. 109:1789-1813.
9. Volk DW, Austin MC, Pierri JN, Sampson AR, Lewis DA (2000): Decreased glutamic acid decarboxylase67 messenger RNA expression in a subset of prefrontal cortical gamma-aminobutyric acid neurons in subjects with schizophrenia. *Arch Gen Psychiatry*. 57:237-245.
10. Hashimoto T, Volk DW, Eggan SM, Mirnics K, Pierri JN, Sun Z, et al. (2003): Gene expression deficits in a subclass of GABA neurons in the prefrontal cortex of subjects with schizophrenia. *J Neurosci*. 23:6315-6326.
11. Woo TU, Whitehead RE, Melchitzky DS, Lewis DA (1998): A subclass of prefrontal gamma-aminobutyric acid axon terminals are selectively altered in schizophrenia. *Proc Natl Acad Sci U S A*. 95:5341-5346.
12. Potkin SG, Turner JA, Brown GG, McCarthy G, Greve DN, Glover GH, et al. (2009): Working memory and DLPFC inefficiency in schizophrenia: the FBIRN study. *Schizophr Bull*. 35:19-31.
13. Naujock M, Speidel A, Fischer S, Kizner V, Dorner-Ciossek C, Gillardon F (2020): Neuronal Differentiation of Induced Pluripotent Stem Cells from Schizophrenia Patients in Two-Dimensional and in Three-Dimensional Cultures Reveals Increased Expression of the Kv4.2 Subunit DPP6 That Contributes to Decreased Neuronal Activity. *Stem Cells Dev*. 29:1577-1587.
14. Chung DW, Fish KN, Lewis DA (2016): Pathological Basis for Deficient Excitatory Drive to Cortical Parvalbumin Interneurons in Schizophrenia. *Am J Psychiatry*. 173:1131-1139.
15. Yang N, Chanda S, Marro S, Ng YH, Janas JA, Haag D, et al. (2017): Generation of pure GABAergic neurons by transcription factor programming. *Nat Methods*. 14:621-628.
16. Rein B, Yan Z (2020): 16p11.2 Copy Number Variations and Neurodevelopmental Disorders. *Trends Neurosci*. 43:886-901.
17. Deshpande A, Yadav S, Dao DQ, Wu ZY, Hokanson KC, Cahill MK, et al. (2017): Cellular Phenotypes in Human iPSC-Derived Neurons from a Genetic Model of Autism Spectrum Disorder. *Cell Rep*. 21:2678-2687.

18. Urresti J, Zhang P, Moran-Losada P, Yu NK, Negraes PD, Trujillo CA, et al. (2021): Cortical organoids model early brain development disrupted by 16p11.2 copy number variants in autism. *Mol Psychiatry*. 26:7560-7580.
19. Sundberg M, Pinson H, Smith RS, Winden KD, Venugopal P, Tai DJC, et al. (2021): 16p11.2 deletion is associated with hyperactivation of human iPSC-derived dopaminergic neuron networks and is rescued by RHOA inhibition in vitro. *Nat Commun*. 12:2897.
20. Glantz LA, Lewis DA (2000): Decreased dendritic spine density on prefrontal cortical pyramidal neurons in schizophrenia. *Arch Gen Psychiatry*. 57:65-73.
21. Glausier JR, Lewis DA (2013): Dendritic spine pathology in schizophrenia. *Neuroscience*. 251:90-107.
22. Brennand KJ, Simone A, Jou J, Gelboin-Burkhart C, Tran N, Sangar S, et al. (2011): Modelling schizophrenia using human induced pluripotent stem cells. *Nature*. 473:221-225.
23. D'Angelo D, Lebon S, Chen Q, Martin-Brevet S, Snyder LG, Hippolyte L, et al. (2016): Defining the Effect of the 16p11.2 Duplication on Cognition, Behavior, and Medical Comorbidities. *JAMA Psychiatry*. 73:20-30.
24. Ochoa S, Usall J, Cobo J, Labad X, Kulkarni J (2012): Gender differences in schizophrenia and first-episode psychosis: a comprehensive literature review. *Schizophr Res Treatment*. 2012:916198.
25. Li R, Ma X, Wang G, Yang J, Wang C (2016): Why sex differences in schizophrenia? *J Transl Neurosci (Beijing)*. 1:37-42.
26. Niarchou M, Chawner S, Doherty JL, Maillard AM, Jacquemont S, Chung WK, et al. (2019): Psychiatric disorders in children with 16p11.2 deletion and duplication. *Transl Psychiatry*. 9:8.
27. Kretz PF, Wagner C, Montillot C, Hugel S, Morella I, Kannan M, et al. (2022): Dissecting the autism-associated 16p11.2 locus identifies multiple drivers in brain phenotypes and unveils a new role for the major vault protein. *bioRxiv*.2022.2001.2023.477432.
28. Dong X, Shen K, Bulow HE (2015): Intrinsic and extrinsic mechanisms of dendritic morphogenesis. *Annu Rev Physiol*. 77:271-300.
29. Lencz T, Yu J, Khan RR, Flaherty E, Carmi S, Lam M, et al. (2021): Novel ultra-rare exonic variants identified in a founder population implicate cadherins in schizophrenia. *Neuron*. 109:1465-1478 e1464.
30. Ward TR, Zhang X, Leung LC, Zhou B, Muench K, Roth JG, et al. (2020): Genome-wide molecular effects of the neuropsychiatric 16p11 CNVs in an iPSC-to-iN neuronal model. *bioRxiv*.2020.2002.2009.940965.
31. Shao Z, Noh H, Bin Kim W, Ni P, Nguyen C, Cote SE, et al. (2019): Dysregulated protocadherin-pathway activity as an intrinsic defect in induced pluripotent stem cell-derived cortical interneurons from subjects with schizophrenia. *Nat Neurosci*. 22:229-242.
32. Schizophrenia Working Group of the Psychiatric Genomics C (2014): Biological insights from 108 schizophrenia-associated genetic loci. *Nature*. 511:421-427.
33. Ripke S, O'Dushlaine C, Chambert K, Moran JL, Kahler AK, Akterin S, et al. (2013): Genome-wide association analysis identifies 13 new risk loci for schizophrenia. *Nat Genet*. 45:1150-1159.
34. Rees E, Carrera N, Morgan J, Hambridge K, Escott-Price V, Pocklington AJ, et al. (2019): Targeted Sequencing of 10,198 Samples Confirms Abnormalities in Neuronal Activity and Implicates Voltage-Gated Sodium Channels in Schizophrenia Pathogenesis. *Biol Psychiatry*. 85:554-562.
35. Fromer M, Pocklington AJ, Kavanagh DH, Williams HJ, Dwyer S, Gormley P, et al. (2014): De novo mutations in schizophrenia implicate synaptic networks. *Nature*. 506:179-184.
36. Vidal-Domenech F, Riquelme G, Pinacho R, Rodriguez-Mias R, Vera A, Monje A, et al. (2020): Calcium-binding proteins are altered in the cerebellum in schizophrenia. *PLoS One*. 15:e0230400.

37. Mudge J, Miller NA, Khrebtukova I, Lindquist IE, May GD, Huntley JJ, et al. (2008): Genomic convergence analysis of schizophrenia: mRNA sequencing reveals altered synaptic vesicular transport in post-mortem cerebellum. *PLoS One*. 3:e3625.
38. Wu JQ, Wang X, Beveridge NJ, Tooney PA, Scott RJ, Carr VJ, et al. (2012): Transcriptome sequencing revealed significant alteration of cortical promoter usage and splicing in schizophrenia. *PLoS One*. 7:e36351.
39. Hamm JP, Shymkiv Y, Mukai J, Gogos JA, Yuste R (2020): Aberrant Cortical Ensembles and Schizophrenia-like Sensory Phenotypes in Setd1a(+/-) Mice. *Biol Psychiatry*. 88:215-223.
40. Hamm JP, Peterka DS, Gogos JA, Yuste R (2017): Altered Cortical Ensembles in Mouse Models of Schizophrenia. *Neuron*. 94:153-167 e158.
41. Sigurdsson T, Stark KL, Karayiorgou M, Gogos JA, Gordon JA (2010): Impaired hippocampal-prefrontal synchrony in a genetic mouse model of schizophrenia. *Nature*. 464:763-767.
42. Earls LR, Bayazitov IT, Fricke RG, Berry RB, Illingworth E, Mittleman G, et al. (2010): Dysregulation of presynaptic calcium and synaptic plasticity in a mouse model of 22q11 deletion syndrome. *J Neurosci*. 30:15843-15855.
43. Khan TA, Revah O, Gordon A, Yoon SJ, Krawisz AK, Goold C, et al. (2020): Neuronal defects in a human cellular model of 22q11.2 deletion syndrome. *Nat Med*. 26:1888-1898.
44. Park SJ, Jeong J, Park YU, Park KS, Lee H, Lee N, et al. (2015): Disrupted-in-schizophrenia-1 (DISC1) Regulates Endoplasmic Reticulum Calcium Dynamics. *Sci Rep*. 5:8694.
45. Grunwald LM, Stock R, Haag K, Buckenmaier S, Eberle MC, Wildgruber D, et al. (2019): Comparative characterization of human induced pluripotent stem cells (hiPSC) derived from patients with schizophrenia and autism. *Transl Psychiatry*. 9:179.
46. Citri A, Malenka RC (2008): Synaptic plasticity: multiple forms, functions, and mechanisms. *Neuropsychopharmacology*. 33:18-41.
47. Li J, Ryan SK, Deboer E, Cook K, Fitzgerald S, Lachman HM, et al. (2019): Mitochondrial deficits in human iPSC-derived neurons from patients with 22q11.2 deletion syndrome and schizophrenia. *Transl Psychiatry*. 9:302.
48. Forrest MP, Parnell E, Penzes P (2018): Dendritic structural plasticity and neuropsychiatric disease. *Nat Rev Neurosci*. 19:215-234.
49. Yao Y, Guo W, Zhang S, Yu H, Yan H, Zhang H, et al. (2021): Cell type-specific and cross-population polygenic risk score analyses of MIR137 gene pathway in schizophrenia. *iScience*. 24:102785.
50. Trubetskoy V, Pardinas AF, Qi T, Panagiotaropoulou G, Awasthi S, Bigdeli TB, et al. (2022): Mapping genomic loci implicates genes and synaptic biology in schizophrenia. *Nature*. 604:502-508.
51. Fruscione F, Valente P, Sterlini B, Romei A, Baldassari S, Fadda M, et al. (2018): PRRT2 controls neuronal excitability by negatively modulating Na+ channel 1.2/1.6 activity. *Brain*. 141:1000-1016.
52. Martin-de-Saavedra MD, Dos Santos M, Culotta L, Varea O, Spielman BP, Parnell E, et al. (2022): Shed CNTNAP2 ectodomain is detectable in CSF and regulates Ca(2+) homeostasis and network synchrony via PMCA2/ATP2B2. *Neuron*. 110:627-643 e629.
53. Dobin A, Davis CA, Schlesinger F, Drenkow J, Zaleski C, Jha S, et al. (2013): STAR: ultrafast universal RNA-seq aligner. *Bioinformatics*. 29:15-21.
54. Anders S, Pyl PT, Huber W (2015): HTSeq--a Python framework to work with high-throughput sequencing data. *Bioinformatics*. 31:166-169.
55. Love MI, Huber W, Anders S (2014): Moderated estimation of fold change and dispersion for RNA-seq data with DESeq2. *Genome Biol*. 15:550.

56. Szklarczyk D, Gable AL, Nastou KC, Lyon D, Kirsch R, Pyysalo S, et al. (2021): The STRING database in 2021: customizable protein-protein networks, and functional characterization of user-uploaded gene/measurement sets. *Nucleic Acids Res*. 49:D605-D612.
57. Huang da W, Sherman BT, Lempicki RA (2009): Systematic and integrative analysis of large gene lists using DAVID bioinformatics resources. *Nat Protoc*. 4:44-57.
58. Koopmans F, van Nierop P, Andres-Alonso M, Byrnes A, Cijsouw T, Coba MP, et al. (2019): SynGO: An Evidence-Based, Expert-Curated Knowledge Base for the Synapse. *Neuron*. 103:217-234 e214.
59. Genovese G, Fromer M, Stahl EA, Ruderfer DM, Chambert K, Landen M, et al. (2016): Increased burden of ultra-rare protein-altering variants among 4,877 individuals with schizophrenia. *Nat Neurosci*. 19:1433-1441.
60. Satterstrom FK, Kosmicki JA, Wang J, Breen MS, De Rubeis S, An JY, et al. (2020): Large-Scale Exome Sequencing Study Implicates Both Developmental and Functional Changes in the Neurobiology of Autism. *Cell*. 180:568-584 e523.
61. Howrigan DP, Rose SA, Samocha KE, Fromer M, Cerrato F, Chen WJ, et al. (2020): Exome sequencing in schizophrenia-affected parent-offspring trios reveals risk conferred by protein-coding de novo mutations. *Nat Neurosci*. 23:185-193.
62. Rees E, Han J, Morgan J, Carrera N, Escott-Price V, Pocklington AJ, et al. (2020): De novo mutations identified by exome sequencing implicate rare missense variants in SLC6A1 in schizophrenia. *Nat Neurosci*. 23:179-184.
63. Wang D, Liu S, Warrell J, Won H, Shi X, Navarro FCP, et al. (2018): Comprehensive functional genomic resource and integrative model for the human brain. *Science*. 362.
64. Mossink B, van Rhijn JR, Wang S, Linda K, Vitale MR, Zoller JEM, et al. (2021): Cadherin-13 is a critical regulator of GABAergic modulation in human stem-cell-derived neuronal networks. *Mol Psychiatry*.
65. Shi J, Levinson DF, Duan J, Sanders AR, Zheng Y, Pe'er I, et al. (2009): Common variants on chromosome 6p22.1 are associated with schizophrenia. *Nature*. 460:753-757.
66. Levinson DF, Duan J, Oh S, Wang K, Sanders AR, Shi J, et al. (2011): Copy number variants in schizophrenia: confirmation of five previous findings and new evidence for 3q29 microdeletions and VIPR2 duplications. *Am J Psychiatry*. 168:302-316.
67. Sanders AR, Levinson DF, Duan J, Dennis JM, Li R, Kendler KS, et al. (2010): The Internet-based MGS2 control sample: self report of mental illness. *Am J Psychiatry*. 167:854-865.
68. Gandal MJ, Haney JR, Parikshak NN, Leppa V, Ramaswami G, Hartl C, et al. (2018): Shared molecular neuropathology across major psychiatric disorders parallels polygenic overlap. *Science*. 359:693-697.
69. Gandal MJ, Zhang P, Hadjimichael E, Walker RL, Chen C, Liu S, et al. (2018): Transcriptome-wide isoform-level dysregulation in ASD, schizophrenia, and bipolar disorder. *Science*. 362.
70. Tai DJ, Ragavendran A, Manavalan P, Stortchevoi A, Seabra CM, Erdin S, et al. (2016): Engineering microdeletions and microduplications by targeting segmental duplications with CRISPR. *Nat Neurosci*. 19:517-522.
71. TR Ward XZ, Louis C. Leung, Bo Zhou, Kristin Muench, Julien G. Roth, Arineh Khechaduri, Melanie J. Plastini, Carol Charlton, Reenal Pattni, Steve Ho, Marcus Ho, Yiling Huang, Joachim F. Hallmayer, Phillippe Mourrain, Theo D. Palmer, Alexander E. Urban (2020): Genome-wide molecular effects of the neuropsychiatric 16p11 CNVs in an iPSC-to-iN neuronal model. bioRxiv
72. Trujillo CA, Gao R, Negraes PD, Gu J, Buchanan J, Preissl S, et al. (2019): Complex Oscillatory Waves Emerging from Cortical Organoids Model Early Human Brain Network Development. *Cell Stem Cell*. 25:558-569 e557.

73. Zhang Y, Pak C, Han Y, Ahlenius H, Zhang Z, Chanda S, et al. (2013): Rapid single-step induction of functional neurons from human pluripotent stem cells. *Neuron*. 78:785-798.
74. Lancaster MA, Knoblich JA (2014): Organogenesis in a dish: modeling development and disease using organoid technologies. *Science*. 345:1247125.
75. Zhang SC, Wernig M, Duncan ID, Brustle O, Thomson JA (2001): In vitro differentiation of transplantable neural precursors from human embryonic stem cells. *Nat Biotechnol*. 19:1129-1133.